Nanoparticle self-assembly: from interactions in suspension to polymer nanocomposites

Anne-Caroline Genix, Julian Oberdisse

Nanoparticle self-assembly: from interactions in suspension to polymer nanocomposites

Anne-Caroline Genix and Julian Oberdisse*

Laboratoire Charles Coulomb (L2C), Université de Montpellier, CNRS, F-34095 Montpellier, France

* Author for correspondence: julian.oberdisse@umontpellier.fr

Abstract

Recent experimental results using in particular small-angle scattering to characterize the self-assembly of mainly hard spherical nanoparticles into higher ordered structures ranging from fractal aggregates to ordered assemblies are reviewed. The crucial control of interparticle interactions is discussed, from chemical surface-modification, or the action of additives like depletion agents, to the generation of directional patches and the use of external fields. It is shown how the properties of interparticle interactions have been used to allow inducing and possibly controlling aggregation, opening the road to the generation of colloidal molecules or potentially metamaterials. In the last part, studies of the microstructure of polymer nanocomposites as an application of volume-spanning and stress-carrying aggregates are discussed.

I. Introduction

It is not always easy to tell nanoparticles (NPs) where to go. The common imperative is to preserve their 'nano-nature', i.e., to keep them individually dispersed, if possible over a long (shelf) life, and thermodynamics of colloidal interactions has taught us how to maintain their colloidal stability using repulsive interactions. Depending on the desired properties or applications, it is necessary to assemble NPs into aggregates, or clusters, or other more organised higher order structures, if possible spontaneously. This requires modifying their interactions in a controlled way. The aim of this review is to highlight recent experimental approaches to chemical and physico-chemical pathways to interactions favouring controlled aggregation and generation of colloidal structures of increasing complexity. Concerning experimental techniques capable of characterizing such NP structures, we have chosen to highlight the benefits of small-angle scattering of neutrons (SANS) and X-rays (SAXS) wherever possible.

Fundamental aspects of this endeavour accompany the results discussed in this article. They are related to understanding interactions between nanoparticles, and how they can be controlled. We discuss the underlying soft matter physics. This starts with tailoring the strength and range of NP interactions in order to control particle assembly. A next possible step is to endow interactions with directionality, either by external fields or through patchiness, enabling an analogy with atoms or molecules, or even macromolecules. One can imagine materials by design, where NPs are structured for example on length-scales comparable to wavelengths of visible light, motivated by the interest for engineering optical bandgaps. Other applications use electronic, magnetic, or quantum properties of nanoparticles, which may be modified by aggregation, opening the road to such applications of controlled NP aggregates. As another important application, we have chosen to concentrate on polymer nanocomposites, the macroscopic properties of which are determined by the assembly of NPs in aggregates and networks of aggregates, structures which are readily characterized by small-angle scattering as well as electron microscopy, in particular transmission electron microscopy (TEM). Our focus is mainly on hard spherical nanoparticles governed by Brownian motion, but some results obtained with microparticles will also be discussed.

Before reviewing recent progress in the field of nanoparticle interactions and aggregation, a basic description of aggregation and of experimental approaches to measuring it is given in section II. The central part of this review (section III) is then organised in three subsections. NPs are usually stabilised in suspension, and the first objective is to destabilise them, inducing aggregation, which is described in the first subsection. Once started, aggregation is difficult to stop, which is why the second subsection focuses on its control. In the last part, finally, a few applications of aggregation are discussed, with particular emphasis on polymer nanocomposites.

II. Nanoparticle aggregates: basic description and experimental determination

This review is about aggregation of nanoparticles, which is why a word on how aggregates can be described, and how we can measure them might be appropriate. First of all, nanoparticles may be of natural (sand dust, metallic oxides, latex) or synthetic origin (gas flame, spray, or more classically precipitation or condensation), see e.g., references [1, 2]. They may be organic or inorganic, and typically studied nanoparticles are (synthetic) latex, gold, silver, and sometimes even diamonds. Other particles are made of more common oxides, like in particular silica, or titanium dioxide.

What we are interested in is the transition from individual NPs, i.e., NPs suspended in some solvent or dispersed in a matrix, like polymer solutions or melts, to a state where NPs touch and stick to each other. Obviously, this is related to the thermodynamics of the systems, including entropic and enthalpic contributions to the total free energy. A tendency towards a new lower-energy state does not mean that the system will reach equilibrium: it might be trapped by energetic barriers in a given state, which may result in kinetically arrested, finite-sized aggregates. While translational or rotational entropy of NPs will always favour disordered states at finite temperature, interactions between particles may be repulsive and stabilising (usually steric or electrostatic), or attractive (like van der Waals forces, electrostatic, depletion, molecular bridging, specific binding of biomolecules, or due to solvophobic properties of the particle surface). [3, 4] One may note that some of these interactions are also of entropic origin, like depletion, where the increase in available configurational space of a depleting agent – usually smaller molecules – is obtained by approaching nanoparticles. In case of high symmetry and monodispersity, the resulting structures may be very regular, and crystallites of various dimensionalities can be formed. In presence of attraction and for large enough concentrations, gels may be formed, i.e. randomly percolating structures conveying mechanical resistance to the sample, whereas at high concentrations, glasses, i.e. out-of-equilibrium structures showing aging phenomena and dynamical arrest may exist, in presence of repulsion or attraction. Anisotropic interactions, finally, may induce a completely new physics, and some examples of creating such interactions using patches are discussed in this review.

If repulsion dominates, one talks of colloidal stability, with the Greek origin of the word colloid (κόλλα, glue) coming from exactly the opposite situation – i.e., stickiness leading to aggregation which is of interest to us here. Once particles stick together, van der Waals forces usually dominate, possibly reinforced by sintering, and aggregation becomes irreversible. An important question is how it can be stopped if aggregates of finite size are desired. Depending on the experimental systems, aggregation may by kinetically arrested, e.g. by a steep increase in sample viscosity, or thermodynamically programmed by the interparticle interactions, which may limit size, e.g. via the number of available bonds, or via a superposition of interaction potentials of different ranges, e.g. short-range attraction combined with long-range electrostatic stabilisation. Sometimes protective

layers may weaken attraction, and reversible clusters, usually called agglomerates, are formed. A large part of this review is thus devoted to how to change interactions, add and shape new ones, including anisotropic interactions, or cancel existing ones.

II.1 Some geometrical aspects of aggregates

While interactions and thermodynamics are the driving forces of aggregation, we focus here on the resulting geometrical structure, in particular as seen by small-angle scattering. This technique is a powerful tool to describe nanoparticle assemblies and correlations both in average and in nanometric detail. [5]

In order to understand the approach, a few simple definitions are needed. We call N_{agg} the average number of nanoparticles which are part of an aggregate, and R_{agg} the typical radius of such an object. Here 'typical' depends on the measurement, for instance one would rather determine hydrodynamic radii in dynamic light scattering (DLS, also called photon correlation spectroscopy), or radii of gyration in static scattering of light, neutrons, or X-rays. If we call the nanoparticle radius a, then the following picture can be drawn:

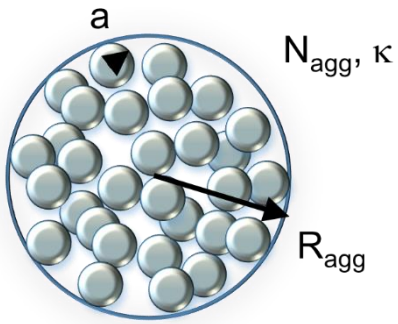

Figure 1: Sketch of an aggregate containing N_{agg} nanoparticles of radius a (possibly polydisperse), of aggregate radius R_{agg}, and internal volume fraction κ.

Based on the radius and the volume of the nanoparticles, one can define [6] one additional parameter, the internal particle volume fraction κ, or compacity, which estimates the volume occupied in the aggregate by the NPs of individual volume $V_0 = 4\pi/3\ a^3$:

$$\kappa = \frac{N_{agg}\, V_0}{\frac{4}{3}\pi\, R_{agg}^3} \qquad (1)$$

One may intuitively expect that the local density is related to the particle coordination number, and to the particle-particle correlation function in general, and this relationship will be presented in the next

subsection. The organisation of the nanoparticles depends on their interactions, as well as on the process of aggregate formation. Unless small crystallites with a regular NP-arrangement on 1D, 2D, or 3D-lattices are formed, aggregates are disordered. Sometimes, they form fractal structures, with a fractal dimension defined via the relationship between N_{agg} and R_{agg}:

$$N_{agg} = \left(\frac{R_{agg}}{a}\right)^{d} \quad (2)$$

Putting together eqs.(1) and (2) shows immediately that aggregates of lower fractal dimension are also on average less dense. Although the density of aggregates is a local microscopic quantity, it may have a direct impact on macroscopic properties. Rheology, e.g., detects the existence of strong stress-carrying paths across a sample. The percolation of nanoparticles may provide such paths, and the space-filling properties of aggregates, and namely the percolation threshold, depend directly on their local density. [7] Note that additional scaling laws different from eq.(2) may be needed to describe the aggregate morphology, like the one relating the minimum path-length to the geometric distance between any two particles, via the tortuosity exponent. [8]

II.2 Experimental approaches

Individual nanoparticles or their suspensions possess measurable properties, and if aggregation changes these properties, they can be used to follow aggregation. Some techniques of optical spectroscopy and in particular plasmon resonance spectroscopy are used in a few articles presented in this review. Rheology, [9, 10] on the other hand, is an indirect technique sensitive to large-scale particle organisation closely related to a prominent application, polymer nanocomposites [11]. Here we mostly focus on direct structural techniques with resolution on the nanoscale, namely small-angle scattering and electron microscopy. As optical microscopy, possibly with 3D resolution using holography [12] or confocal microscopy [13], is usually limited to micron-sized objects, it is therefore excluded from this review.

Electron microscopy, in particular in transmission, is a widely used technique to characterise nanoparticles and their aggregates – in any event much more often than X-ray microscopy [14]. Obvious limitations are however often overlooked, like the 2D-projection of three dimensional objects, and the possibly limited representativity of single pictures. Moreover, when nanoparticles are incorporated in a polymer matrix, the samples can rather safely be cut in thin slices of typically 70 nm thickness, but when the NPs are suspended in a liquid, a non-perturbative view using cryo-techniques becomes more challenging. When suspensions are dried, capillary forces may affect the dispersion, and induce additional aggregation, which was not present in the original suspension. Only a few tomographic approaches with electrons [15] or X-rays [16] have been developed to avoid the projection problem into two dimensions. In particular, Dalmas et al [17] proposed an optimised procedure for the segmentation of

TEM tomograms in order to isolate nanoparticles. Their local environment in polymer nanocomposites was then described via a 3D Voronoi tesselation, giving access to the distribution of local volume fractions in the samples as defined in eq.(1). Legg et al [18] used cryo-TEM-based tomography to retrieve the mass autocorrelation function of ferrihydrate nanoparticles in water. This function can be directly compared to results of small-angle scattering, namely the fractal dimension, thus emphasizing the complementarity of both methods. One may cite other complementary approaches, including automated image analysis. [19] For example, we have used TEM to count aggregation numbers in polymer nanocomposites, and checked our statistics by aggregate reconstruction and comparing their Fourier transform to measured small-angle scattering. [20] Jouault et al have studied aggregation numbers and deformation in a stretched nanocomposite. [21] To finish this paragraph on electron microscopy, the contribution of simulation methods to 2D-image analysis of three dimensional aggregates may also be mentioned. [22] In their article, Häbel et al further develop a statistical analysis of experimental microscopy images of aggregating silica gels, based on a simulation of the cluster aggregation process, followed by generation of simulated micrographs, and their comparison to experiments using statistical summary functions. In the end, this allows concluding on interaction potentials between nanoparticles, while reducing measurement artefacts due to the two dimensional nature of the pictures.

Besides dynamic light scattering, which can be used in-situ as long as one stays at low enough concentrations, small-angle scattering of light, neutrons, or X-rays are heavily used for the characterisation of nanoparticles and aggregates. If needed, some textbooks and reviews can be recommended, including freely available lecture series. [5, 23, 24] One of the main advantages of these techniques is the ensemble average, which is performed over a macroscopic piece of sample illuminated by the beam, while keeping nanometric resolution, expressed by the range of the scattering wave vector q, usually between some 10^{-4} and 0.5 $Å^{-1}$. The inverse of q expresses the length scale probed in a scattering experiment, thus from roughly a fraction of a nanometer up to a micron. The scattered intensity is usually denoted I(q), the differential scattering cross section per unit sample volume, expressing the scattering probability in a given direction, per unit solid angle. A coherent scattering intensity arises from nano-structured matter with contrast, i.e., a difference in scattering length density, a quantity describing the scattering power of material. In X-ray scattering, for example, an electron-dense zone has contrast (and thus scatters) with respect to less electron-dense zones around. In other words, chemical differences are visible in scattering. Moreover, in neutron (and also anomalous X-ray) scattering, the contrast can be tuned via isotopic substitution. For example, a deuterated polymer particle has a different visibility than the otherwise chemically identical protonated polymer particle. This property may one day come in handy to differentiate multi-pod structures to be discussed later in this review, and measure partial correlations between particles.

The scattered small-angle intensity is usually broken down in a form factor contribution P(q), which describes the shape of individual NPs, and a structure factor S(q). This works strictly speaking only for monodisperse objects of spherical symmetry, where one can separate the two terms in a product:

$$I(q) = A\, P(q)\, S(q) \tag{3}$$

The prefactor A takes concentration, particle volume, and scattering contrast into account. There are as many functional forms of S(q) and P(q) as there are interactions and particle shapes. In most publications on suspended nanoparticle assemblies, expressions or numerical calculations of S(q) based on the theory of simple liquids are used. [25] This includes a possibly numerical resolution of an integral equation called the Ornstein-Zernike equation, which needs a suitable, potential-dependent closure, which in the end gives the name to the corresponding structure factor. [26] In common cases of repulsive interparticle potentials, it boils down to either hard-sphere repulsion described by the Percus-Yevick structure factor for short-range repulsion, [27] or Yukawa-type structure factors accounting for long-range repulsion, typically of electrostatic origin [28, 29]. Structure factors arising from attractive potentials may also be described. In presence of short-ranged attractive wells at the particle surface, forming so-called “sticky beads”, a well-known S(q) is the Baxter structure factor [30]. Once the particles really build aggregates, one usually needs numerical simulations to describe a specific geometry. [31] There exists however at least one simple case, fractals. Aggregates of fractal dimension d possess a power-law correlation function with exponent (d - 3), [32, 33] and their structure factor follows a power-law

$$S(q) \propto 1/q^{d} \tag{4}$$

This law is valid on scales ranging from the total size of the fractal down to the size of the building unit. Alternatively, the range where eq.(4) is found to hold is delimited by the inverse of aggregate size and the inverse of particle size. It is thus possible to read off the fractal dimension d from the slope of the intensity, the particle form factor being constant in this range. There have been attempts to define universality classes identified by different fractal dimensions, as typically encountered in diffusion- or reaction-limited aggregation, as well as in aggregation of clusters. [34] Several expressions for the scattering of finite-sized fractals exist, combining a low-q Guinier description of aggregate size with a fractal law as given in eq.(4). [32, 33, 35, 36] Several fractal regimes can co-exist on different scales. In real space, they correspond to aggregates of a given size and internal fractality, which assemble on a large scale, with a different fractal dimension. Such a feature can be captured by the unified law by Beaucage [37, 38]. Naturally, multiple structures on different length scales are right in the focus of hierarchical structures, the simplest one being single aggregates.

In order to observe fractality, however, a large experimental q-range is needed, usually based on various 'U' or 'V' (for ultra-, or very-) SANS or SAXS experiments, [39-43] or very small-angle options on existing instruments, like D11 [44] at ILL or beamline ID2 [45] at ESRF (Grenoble, France). A completely different approach has been developed by a group at the research reactor in Delft, based on spin-echo SANS. [46] This technique uses the spin of the neutron to encode the scattering angles, reaching very high resolution and thus large real-space scales, up to many microns. Moreover, in analogy with neutron spin echo used for quasi-elastic scattering, the resulting function is already transformed in real space. The authors have applied this method to fluidized TiO_2-nanoparticles, and their multi-fractal nature can be appreciated in Figure 2.

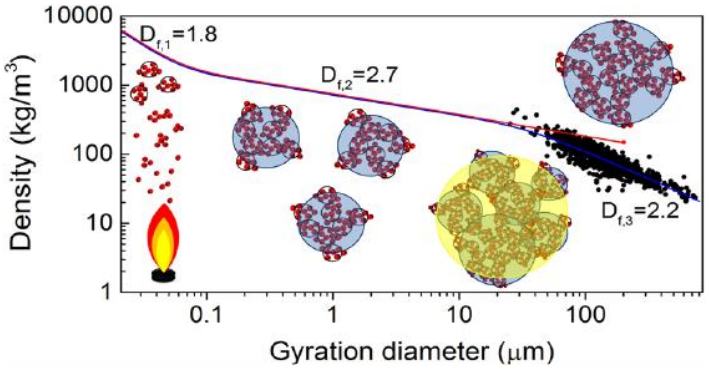

Figure 2: The density of aggregates as a function of their diameter of gyration as obtained by spin-echo SANS by de Martin et al. [46] Reproduced with permission from [46]. Copyright (2014) American Chemical Society.

One of the problems related to scattering is the smoothing of the signal due to polydispersity. It is actually worse than this, because polydispersity in particle size and shape makes eq.(3) fail. This is due to the presence of multiple structure factors (called partial structure factors) between all particles of different sizes. In numerical calculations, the correct terms summing up all the correlations may be accounted for, but this is not often used by experimentalists.

There is one case where we have performed simulations on interactions between polydisperse particles, and parametrised the results. The concept was first applied in an article of Baeza et al, [6] and then generalized by us [47]. The local particle density κ, which depends on the correlations between nanoparticles inside aggregates can be read off directly from a measured intensity. The underlying idea is that higher local coordination induces a depression of the intensity, termed the correlation hole, and we have proposed a mapping of this depression on κ, for arbitrary polydispersity. In practice, one has to measure the particle form factor P(q) in order to know the polydispersity, and then determine the depth of the correlation hole by dividing I(q) by P(q). The value of the apparent structure factor in the dip, S_0, is directly related to the compacity κ via the following equation [6, 47]

$$S_0 = \frac{(1-\alpha\kappa)^4}{(1+2\alpha\kappa)^2} \qquad (5)$$

where α is a parameter, which depends on particle polydispersity. α is given by an explicit expression obtained from numerical simulations in ref [47]. In other cases, complete numerical calculations helped to determine the distribution of aggregate sizes, [48] or the cross-check of experimentally determined aggregate-mass distributions from image analysis of TEM pictures with the scattered intensity [20].

Finally, more sophisticated scattering techniques should also be mentioned, in particular grazing-incidence small-angle scattering, GISAS. [49] This technique gives access to particle correlations in a surface layer, and therefore gives reciprocal-space information comparable to (real-space) atomic force microscopy (AFM), as proposed by Le Diagon et al [50] on particles in nanocomposites some time ago.

III. Controlled nanoparticle structures of increasing complexity

There is a strong on-going research activity on nanoparticles and their aggregation. Our view is focused on bottom-up approaches, i.e., based on spontaneous self-assembly. This section is subdivided in three subsections, entitled "Inducing aggregation", "Controlling aggregation", and "From aggregation to applications", respectively. While the first part deals with the many thermodynamic tricks to make particles aggregate, the second one reports on experiments trying to stop aggregation at some stage. This is closely related to limiting the effect of attractive interactions, which brings us naturally to patchiness of nanoparticles, but not only. In the last part, finally, we discuss various applications, with a particular focus on polymer nanocomposites – a field where fundamental understanding of aggregation has direct consequences on industrial applications.

III.1 Inducing aggregation

Once pure nanoparticles are dried, strong attractive forces and possibly sintering make it often impossible to redisperse them in a solvent, unless high amounts of energy are added, e.g., by shearing. Sometimes they can be redispersed, like for instance nanodiamonds, which form stable fractal clusters resisting drying. [51] In general, however, NPs need to be stabilized to be sold in suspension, by adding one of the repulsive potentials mentioned in section II, or alternatively, they may be stabilized sterically, and then dried. After redispersion in a solvent or matrix, they are thus stabilized, and the first path to induce aggregation is to somehow cancel the added repulsive potential.

The simplest way to do so is to weaken electrostatic repulsion by either changing the electrostatic charge on each particle if it is pH-dependent, or by decreasing the Debye screening length by adding salt, see for example [52]. Influencing the solubility of adsorbed or grafted polymer chains ensuring dispersion of NPs is the equivalent approach for steric stabilisation. Zhang et al [53] have prepared poly(ethylene glycol)-stabilised gold nanoparticles, termed Au-PEG (6 kg/mol), and regulated the

steric interactions by adding salt, thereby changing the solvent conditions for PEG in water, exploiting the well-known phase behaviour of PEG. In particular, PEG is known to possess a lower critical solution temperature (LCST), above which it becomes insoluble in water. [54] While the polymer brush in Θ- or good solvent conditions is hydrated and opposes entropic forces to compression, the layer shrinks in bad solvent conditions, and becomes sticky due to the effective surface tension between the layer and the solvent. As a result, the particles crystallize, with beautiful FCC structure factor peaks growing as a function of K_2CO_3 content. This experiment illustrates that it is easy to trigger aggregation, but difficult to avoid the formation of a second, here completely crystallized, phase. For comparison, an application of the same idea was published by Babayan et al in 2010. [55] Using SANS and TEM, they have described the formation of locally linear silica aggregates generated by decreasing the solubility of adsorbed PEG (sometimes named PEO, for poly(ethylene oxide)) with increasing temperature, and other polymers which display a LCST. The directionality of the interaction is generated by keeping long-range electrostatic repulsion, and permanent aggregates can be obtained by consolidation through preferential adsorption of silicates in the NP contact area, at high temperature. At high heating times, branching and finally phase separation are observed.

Instead of modifying the parameters of a given interaction potential, one may also make use of the hydro- or solvophobic properties of NP surfaces in order to manipulate structure formation through the resulting interaction potential. Most inorganic NPs are intrinsically hydrophilic, due to the existence of electrostatic charges, like those stemming from silanol (Si-OH) groups on the surface of silica NPs, depending on pH. These particles are thus spontaneously well dispersed in water. Changing such hydrophilic surfaces into hydrophobic ones can be done by surface modification, either using surfactant adsorption, or chemical reactions with small hydrophobic molecules. Surfactant adsorption and its impact on nanoparticle aggregation have been studied extensively by many different groups in the past. Aswal and Kohlbrecher [56] have proposed SANS experiments using contrast variation to highlight either the surfactant micelles or the NPs. In this article, they have studied non-ionic micelles, which adsorb [57, 58] and provide steric stabilisation to the NPs in addition to not decreasing the charges. When anionic or cationic surfactants are added to the NPs, only the latter induce aggregation due to adsorption and screening of electrostatics, without changing their micellar morphology. As a result, fractal aggregates are formed, and scattering gives direct access to the fractal dimension, 2.3 in this case.

Coming back to chemical surface modification, an illustrative example is given by Moro et al, [59] who hydrophobise silica NPs with organosilanes directly in water, and study the response of these particles to drying. Evaporating the aqueous solvent has the obvious consequence of concentrating the NPs, and depending on the silanisation, and in particular the grafting density, they organise differently in space, as can be seen by cryo-TEM and SAXS in Figure 3. The resulting structure factors directly show that hydrophobisation promotes aggregation in the aqueous phase, in a controlled way, and the NP

dispersion can be followed at arbitrary concentrations during drying, a key advantage of scattering. The increase in aggregation with surface grafting is accompanied by a low-q upturn in the scattering in Figure 3e. From the rather low resulting fractal dimension one can conclude on the tenuous nature of the aggregates, which is confirmed by the absence of a correlation hole. Higher pre-aggregation in suspension induces heterogeneities leading to final materials becoming more porous, while the hydrophobisation reduces water uptake. While grafting organosilane clearly aims at hydrophobic interactions, additional attractive interactions may be generated by peptoids, which are peptide mimics, i.e., biomimetic oligomers like N-substituted glycines. These molecules interact in particular via phenol-group induced π-π-stacking, i.e., non-covalent attractive force caused by electrostatic interactions between aromatic rings. Their effect on metal particle assembly was studied by Tigger-Zaborov and Mayaan recently. [60] They clearly observe very small clusters of finite size, with a mass dependence on the type and length of the peptoid. At this stage, however, the reasons for the size limitations remain to be elucidated.

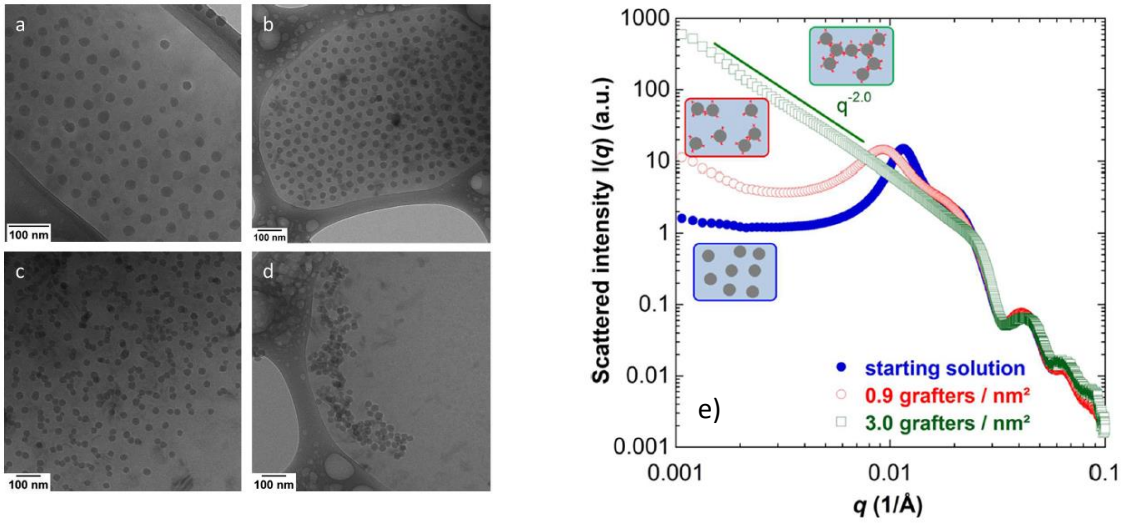

Figure 3: (a-d) Cryo-TEM pictures of silanized nanoparticles in aqueous suspension at increasing grafting density (0, 0.7, 0.9, and 3 nm^{-2}) by Moro et al. [59] **(e)** Corresponding SAXS intensities. Reproduced with permission from [59]. Copyright (2017) American Chemical Society.

The surface modification-route has been used by us in order to control NP aggregation in suspension, and ultimately in polymer nanocomposites, as discussed in the last part of this review. Hydrophobisation in water of alumina-coated silica NPs with phosphonic acids of various hydrophobicity has been performed by Schmitt-Pauly et al, [61] and the resulting aggregates studied by DLS, small-angle scattering, and TEM of dried suspensions. Hydrophilic short diethylene glycol grafts were found to successfully preserve colloidal stability up to a high grafting density of 3 nm^{-2}. More hydrophobic grafts, from C_3 to C_8-alkyl groups, progressively favoured aggregation, while surprisingly a carboxyl-terminated graft also did so, presumably due to a folded-back conformation exposing its hydrophobic methylene groups. In a second experiment, TiO_2 nanoparticles have been

modified, using a phase transfer from water to organic solvents, in particular chloroform. [62] In such systems, it is rare to encounter completely dispersed NPs, but rather small primary aggregates. The original result of this study is that the aggregation after transfer was independent of the aggregation state of the NPs before, i.e., in water, where aggregation could be induced by addition of salt or changes in pH. The phase transfer with simultaneous grafting produced thus rather small aggregates of NPs surrounded by a homogeneous grafted layer, as shown by SANS.

The addition of stabilisers may sometimes be a part of the synthesis protocol, like citrate molecules used as capping agent of silver NPs by Affonso de Oliviera et al. [63] These authors have studied the influence of the amount of a reducing and thus NP-forming agent, sodium borohydrate, on the NP formation and aggregation. As evidenced by a low-q increase in SAXS – which is unfortunately rather featureless –, the electrostatic competition of the reducing agent with the NP-stabilising citrate induces chain-like structures at low concentrations. This appears to be followed by the formation of large polydisperse aggregates at high concentrations.

Slow aggregation of citrate-stabilized NPs has been triggered by addition of cysteine, an amino-mercapto acid, by Jiang et al. [64] This molecule competes with the citrate, and its surface modification results in time-dependent aggregation. The authors have used particle tracking to investigate diffusion, and thus the effective aggregate radius via the Stokes-Einstein equation, in analogy with dynamic light scattering. TEM indicate the formation of linear or bifurcating particle chains, which is explained by the enhanced anisotropy due to Au-S bonds. Optical properties are studied by UV-vis, showing two peaks, one of which is due to the growing aggregates.

Nanoparticles can be linked directly with molecules capable of grafting on both ends, as done with silver nanoparticles and short aliphatic chains bifunctionalized with thiols by Izquierdo-Lorenzo et al. [65] These authors have followed the coupling of plasmon modes of close-by, thus aggregating NPs, whereas aggregation itself is shown by TEM to be mainly linear at low, and to evolve into large clusters at higher linker concentration.

Attractive potentials can also be generated by adding objects which are smaller than the nanoparticles, and which interact repulsively, leading to depletion interaction between the bigger particles. This is an entropic effect based on the overlap of excluded volumes. Ray, Aswal and Kohlbrecher have presented an intuitive example, where non-ionic micelles are first adsorbed, without impacting the colloidal stability, and then desorbed by adding salt. [66] This leads to aggregation, which is easily picked up by the low-angle increase in SANS, as well as the prominent particle-particle peak showing close contact between nearest neighbours.

Replacing surfactants by globular proteins has attracted considerable attention in the community, and much of the physics can be played in an analogous way with such biomolecules. To start with, protein adsorption on silica nanoparticles has been studied extensively, in particular β-lactoglobuline, and

lysozyme, two model proteins. [67] Adding such globular proteins to a silica suspension induces aggregation. Yadav et al [68, 69] have compared the effect of adsorbing lysozyme, which modifies the electrostatic charge of the particles, and bovine serum albumin (BSA), which does not adsorb, and therefore causes depletion interaction, using a combination of SANS and turbidity measurements. Once lysozyme sticks to the NP surface, it can stick to another available NP surface, and thus bridge particles. This idea of protein-induced aggregation has been further investigated by Barthi et al. [70] In particular, they discuss the availability of the most positively charged sites on the proteins, on opposite sides of it. In their analysis of the scattered intensities, they identify the pH- and electrolyte-concentrations inducing the strongest bridging interaction, described by an attractive square-well potential.

To finish this discussion of nanoparticle aggregation in presence of proteins and surfactants, it may be noted that the combination of both has been studied by Mehan et al. [71] These authors use SANS and contrast matching to analyse the total structure, and compare it to the one of binary subsets. For instance, they show that anionic protein-surfactant complexes can provoke NP aggregation even if the pure protein carries electrostatic charge of the same sign as the silica NPs, and acts as a non-adsorbing depletion agent in the binary system with particles. The resulting structure is fractal, and the density of the fractals (i.e., the dimension, here typically > 2.5) can be varied via the formulation.

It is only a small step from protein-induced aggregation to the effect of polymers. As with proteins, the field is large, due to the many possible interactions that can be mediated by macromolecules. We start again with depletion, which depends only on the smaller size and the non-adsorbing properties. Aggregation induced by free and neutral PEG-molecules has been shown by Kumar et al [72, 73] to set in as soon as electrostatic stabilisation is sufficiently weakened, which is why the observation depends on the electrolyte concentration. Indeed, the low-angle intensity highlighting NP aggregation increases first moderately with salt, indicating rather small-aggregates. At higher salt concentration, the data follow a power-law without observable finite-size cut-off, indicating the formation of large and dense assemblies, with nearest neighbour correlations expressed by a correlation hole, and the signature of surface fractals.

As soon as the added macromolecules bear additional properties, new physics can be developed. If they are charged, i.e., polyelectrolytes, they can induce aggregation by bridging NPs of opposite electrostatic charge. This has been studied for magnesium hydroxide nanoparticles using TEM and in particular light scattering by Li et al. [74] Via static light scattering, they find aggregates with a fractal dimension of 2.2, which is compatible with reaction-limited cluster aggregation. Moreover, they follow kinetics with DLS, relating the aggregate-size increase with time to a collision efficiency, and put forward a possible explanation of their observations through heterogeneous adsorption, i.e., patches. Moreover, using rheology, they show different viscoelastic regimes of the flocs, depending on

the concentration of magnesium, which are related either to bridging, or to depletion interactions, both induced by the polyelectrolyte.

Instead of complexing nanoparticles with synthetic polyelectrolytes, a similar result can be obtained with natural ones, like polysaccharides. The aim of such approaches is to vary the stiffness of the macromolecules, synthetic molecules being usually considerably more flexible. Shi et al [75] have proposed a combined SAXS-SANS and cryo-TEM study of the formation of silica aggregates obtained when adding chitosan, a linear cationic polysaccharide of measured persistence length 9 nm, which is comparable to the NP radius. The analysis of the scattering patterns in excess of NPs shows that this leads to the formation of stiff linear chains of finite-size (ca. 15 particles), whereas a comparable synthetic polyelectrolyte – poly(L-lysine) – generates bigger and denser aggregates, i.e., of higher fractal dimension.

Co-assembling objects of opposite charge is of course not restricted to polyelectrolytes. An example of the hetero-aggregation of mixtures of oppositely charged nanoparticles into binary crystals has been published more than ten years ago. [76] Without focusing on aggregate geometries, aggregation rate constants of particle mixtures have been estimated by light scattering techniques. [77] This hetero-aggregation route is also the starting point for stabilising chains and clusters formed in presence of electric fields [78] as discussed in the next section.

In this subsection, we have presented selected pathways to induce aggregation in colloidal systems in a systematic way. In some cases, large-scale gelation or crystallisation was reported, while others led to the formation of finite-sized particle assemblies. The physical mechanisms of the origin of these differences are a priori unclear, once attractive interactions have taken control. In the next subsection, we will discuss how one can win back control.

III.2 Controlling aggregation

Once aggregation is induced, why would it stop? Continuing aggregation of particles usually leads to phase separation due to density mismatch and sedimentation. In some cases, crystallisation is induced, if particle shapes, monodispersity, and interactions are compatible with crystalline order. [79] In this case, symmetry-revealing Bragg-peaks are usually visible in scattering, growing in intensity and refining in width as the crystallites grow. So how can one limit aggregation? There is a range of possibilities, and the first one is Brownian motion: an aggregated state being more ordered, entropy naturally favours redispersion. As a second aggregation-limiting effect, repulsive forces may be present. They may act over long distances, like electrostatics in aqueous suspensions, keeping particles far away from contact. Alternatively, short-range potentials, in particular of steric origin, may let particles approach but prevent close-contact, which would lead to irreversible clustering due to van der Waals forces. In some cases, such repulsive forces are weak for the single particle, and build up

progressively with aggregation, like steric layers becoming denser with aggregate growth. Let us also note that this does not have to happen at thermal equilibrium, and that kinetically trapped states of aggregation may form just the desired cluster size. Finally, one prominent pathway is to limit the attractive forces themselves, in particular angularly. Directionality in the interactions may be introduced either by physico-chemical means, i.e., be intrinsically attached to the particles ("patches"), or by external fields. Both will be discussed below.

One of the first polymer-routes to simultaneously initiate and limit aggregation was popularized some 15 years ago by J.-F. Berret and co-workers, and reviewed in 2011. [80] The underlying idea is based on a diblock copolymer chemistry, with one hydrophilic neutral block, and a – usually shorter – polyelectrolyte of charge opposite to the nanoparticles to be assembled. Surprisingly at first sight, this double-hydrophilic polymer induces aggregation via complexation of the NPs by the polyelectrolyte, which leads to bridging, but limits aggregation by forming a hydrophilic corona playing the role of a steric stabiliser of the complex, coined 'complex colloid'. The core-corona structure has been extensively studied by combinations of light scattering – the hydrodynamic radius being sensitive to the 'hairy' corona –, and SANS characterizing the dense core filled with nanoparticles, or even micelles. This approach has then been generalized, as reviewed in ref [81].

In the previous subsection, aggregation was shown to be potentially induced by hydrophobisation of nanoparticles. Recently, Jang et al [82] have introduced a second, hydrophilic ligand, and could show by DLS and TEM that rather small and well-controlled gold aggregates can be obtained. They rationalise this observation with a mechanism similar to the one at work in complex colloids: the hydrophobic ligands induce aggregation, and displace the hydrophilic ones to the surface of the aggregates, thereby generating a repulsive and thus stabilising potential.

Also in the previous subsection, we have discussed assemblies of particles of opposite charge, which usually grow without control into very large structures. By carefully varying the surface charge of a binary mixture of a priori negative particles by adsorption of an oppositely charged surfactant, Nakamura et al [83] succeed in creating the conditions of opposite charges for self-assembling nanoparticles in a controlled way. By changing the concentration and type of the particles, the strength of the electrostatic interaction and resulting aggregation could be tuned, leading to distributions of isolated clusters of a few particles. These authors report a wide cluster size distribution obtained from optical micrographs, and propose to use fractionation to reduce polydispersity.

Controlling attractive potentials by reducing the available attractive area on nanoparticles has become the starting point of an entire new sub-discipline, patchy particles. This is due to the combination of several features and developments. Among the more important ones, one may cite the experimental availability of different types of patchiness over the past ten years. Next, simulations have accompanied experimental observations, providing a conceptual framework, see for example the

review by Gârlea et al on the assembly of soft patchy nanoparticles. [84] The perspective by Bianchi et al et is separated in top-down – mostly leading to hard particles – and bottom-up (mainly soft, with flexible particles and bonding patterns, based on polymer and biopolymer-induced bonding) approaches to form patchy NPs with the goal to limit the valence. [85] Concerning properties, symmetry-breaking by patchiness allows shaping attraction, possibly pre-programming it, [86] in order to build low-coordination structures, as opposed to isotropically attractive NPs, which maximise the number of neighbours. Mimicking atomic orbitals, colloidal molecules, which can then be assembled on larger scales, also belong to this class of structures. Clearly, the available parameter space, in terms of type of interactions – from simply solvophobic to specific complementary binding using deoxyribonucleic acid (DNA) –, as well as in terms of number and directions of patches – starting with the double-faced Janus – opens new horizons in colloidal interactions.

It is not the aim of the present review to discuss the synthesis and applications of patchy particles in detail – much more exhaustive reviews on recent advances exist. [87, 88] Instead, we focus on experimental studies where patchiness was used to control or limit the available "aggregation space". Although scattering would be well-suited for structural studies, in particular neutron scattering with contrast variation allowing the determination of correlations between patches, and between particles inside colloidal assemblies, particle sizes usually approach the micron, and optical microscopy and its variants are the methods of choice, and sometimes electron microscopy.

Janus particles are a natural starting point for this discussion. A recent example of synthesis based on two incompatible polymers, a pod of soft acrylate (low T_g) positioned on a hard polystyrene (PS, high T_g) bead by Skelhon et al.[89] These particles are initially sterically stabilised, but the adsorbed stabilising molecule can be removed by dilution. Then, collisions between the soft viscous polymer parts induce merging and thus sticking of the particles, followed by local reconfiguration in order to decrease the surface energy. The authors have observed the formation of symmetric particle assemblies, e.g., tetrahedral symmetry for four particles, and also higher-order clusters. It is difficult, however, to imagine the formation of any extended structure, due to the exclusively soft-soft attraction. Janus particles are often formed at interfaces, where they can be selectively functionalized, "from below" or "from above". Sabapathy et al [90] report on the synthesis of non-spherical functionalized microparticles, which are deformed at an oil-water interface by heterogeneous swelling. Due to the different curvatures on each particle side, a chain-like or micelle-like assembly is observed by optical microscopy, depending on the shape of the NPs.

Polymer particles are not the only ones which have been synthesised, and one can follow the versatile self-assembly strategy proposed by Gschneidtner et al [91] to form colloidal heterodimers, made of two particles of different noble metals. These authors show by DLS and TEM that they have succeeded to produce metallic dimers by electrostatic attraction between non identical particles, while carefully controlling experimental conditions, in particular particle and ligand concentrations in order to limit

the formation of multimers. Moreover, they provide a proof-of-principle hydrogen sensing experiment on a single Au-Pd heterodimer, the palladium reacting with hydrogen and shifting the plasmonic response of the gold NP.

Bifunctionality naturally favours the formation of chains. Pushing further the analogy with the chemistry of polymerisation, Klinkova et al [92] have studied the linear aggregation of gold nanorods functionalized with polystyrene at each end, in presence of colloidal chain stoppers, i.e., monofunctional colloids which impede the polymerisation reaction by sticking to the reactive end of a chain of particles. In particular, they successfully showed and modelled that the linear growth in time of chain length in absence of stoppers is suppressed as the latter are added. In this context, it may be noticed that small-angle scattering has been decisive in characterising the conformation of polymer molecules, as it directly translates the statistical properties of ensembles of (possibly branched) chains into power laws in q-space of high statistical relevance. We hope that a similar application will elucidate the conformational properties of colloidal polymers, or "nanopolymers". [93]

The effect of changing the "valency" from Janus-particles to higher valency has been nicely illustrated in the work by Schreiber et al. [94] These authors control the bonding symmetry of DNA-modified gold particles, using exactly positioned complementary linker oligonucleotides, as shown in Figure 4. This important synthetic effort allows a spectacular control of aggregation, from one-dimensional, chain-like aggregates built with particles with two bonds on opposite sites, to square-like 2D-lattices constructed with particles with four in-plane bonds at 90°, and finally a hexagonal network with the appropriate bonding angles. With the availability of such a chemistry, one could imagine size control by mixing particles with appropriate bonds, for example of lower valency acting as stoppers.

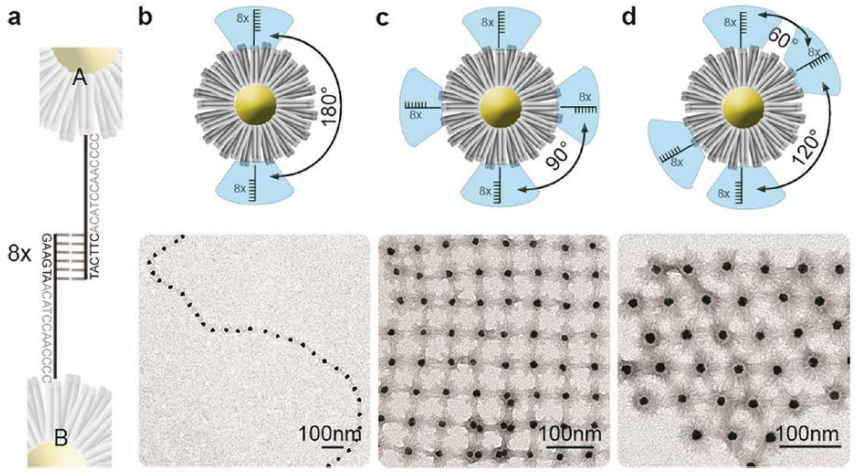

Figure 4: (a) Molecular hybridisation scheme. **(b-d)** Different hybridisation geometries, with corresponding lattices below, by Schreiber et al. [94] Reproduced with permission from [94]. Copyright (2016) American Chemical Society.

Note that DNA-recognition has also been introduced not only to assemble, but also to disassemble gold NPs in suspension by addition of a target oligonucleotide, as shown by DLS, TEM, and optical properties by Trantakis et al. [95] These authors have thus made use of a general property of DNA bonding, which is reversible and temperature-controlled. [96]

Directionality of bonds is a key property related to patches, as it governs coordination. As we have just seen, *specificity* of the bonds can be designed using oligonucleotides. Designing materials by assembling particles with complementary DNA strands, thus making use of base-pairing, is a very active field, which has been recently reviewed by Rogers et al, [97] with a particular emphasis on the formation of colloidal crystals. Such interactions can be combined with particle anisotropy, as shown by Lu et al. [98] They report on the formation of superlattices, like binary cube-sphere assemblies, with electron microscopy to show the local structure, and SAXS to prove long-range order. Alternatively, Wang et al [99] have shown in 2012 that patchy particles can be produced by swelling and post-polymerization of precursor aggregates with, e.g., styrene. Such a route leaves some protrusions as patches, which could be decorated with oligonucleotides in order to combine specificity and directionality of the bonds. Based on different swelling behaviour of the polystyrene patches and the particle shell, the same group recently designed shape-shifting patchy particles with a transition from initially convex to concave patches. [100] Such swelling characteristics provide an interesting path towards the formation of site-specific self-assemblies via surface-liquid capillary bridging. Similar approaches in tailoring the directionality of the patches have been pioneered by groups in Bordeaux, see for example [101]. Based on colloidal multipods made of different materials, namely silica and (dissolvable) polymer, they have produced tetra-, hexa- and dodecavalent particles with notches left after dissolving the polymer, see Figure 5 for illustration. Moreover, incomplete dissolution leaves some organic material at the patches, which can be used for further functionalisation. To summarize, it is now possible to combine specificity with directionality, paving the way to any type of "colloidal lego", using e.g., recently developed multicavity particles, which can reversibly bridge with any complementary shape particles via depletion interactions. [102]

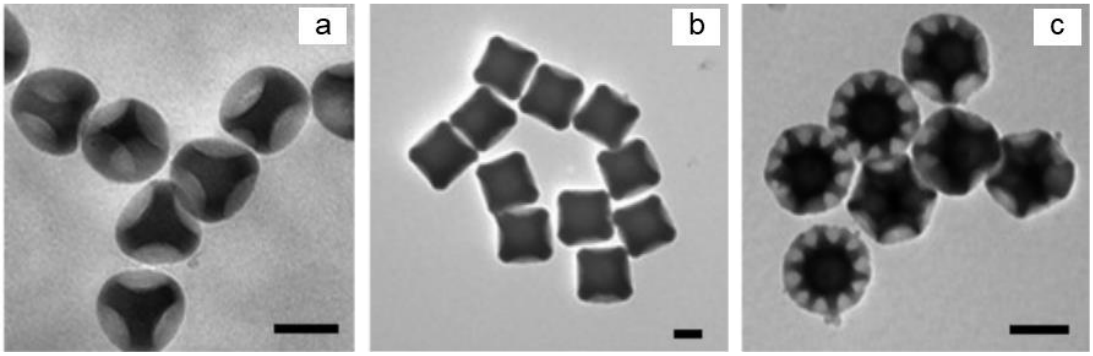

Figure 5: High-magnification TEM images of tetravalent (a), hexavalent (b), and dodecavalent (c) silica particles. Scale bar: 100 nm by Désert et al. [101] Reproduced and adapted with permission from [101]. Copyright (2013) Wiley-VCH.

A completely different route to multi-valent nanoparticles has been explored by Choueiri et al. [103] They have taken advantage of a reduction in solvent quality to induce the local concentration of otherwise homogeneous polymer brushes on NPs. These patches can not only be made irreversible by polymerisation, but the patterned nanoparticles display remarkable self-assembly properties.

Up to now, we have reviewed ways to encode a desired assembly in the shape and interactions between nanoparticles. Particle assembly can also be guided externally, e.g., by patterned surfaces. We deliberately ignore this approach here, as well as capillarity-guided aggregation of particles on fluid surfaces (see for instance [104, 105]), as we focus on dispersed systems. Let us simply note that such patterns may be of importance for plasmonic NPs needing a high regularity in interparticle spacing. [106]

The use of external fields to guide NPs is another route to design assemblies. These fields may be of various natures, as reviewed already some years ago by Grzelczak et al. [107] These authors insist on the fact that in-situ measurements, in particular using SANS [108] or SAXS, are able to contribute to a thorough characterisation of average structural properties of nanoparticle assemblies in any type of fields, including flow and shear. Flow-SANS measurements using a Couette shear cell have been performed on colloidal hard-sphere suspensions. [109, 110] It allowed for a direct observation of hydroclusters, i.e., density fluctuations of particles under flow, [109] whereas anisotropic microstructures were evidenced with preferential orientation along both the neutral and compression axis of flow in a system with short-range attractions [110]. An example of the use of shear and light scattering has been recently reported by Meng et al. [111] The underlying idea is quite simple: shear favours particle collisions, and by shearing binary mixtures of particles of different colloidal stability, it is possible to entrap one type of NP within clusters of the other type. Large micron-sized clusters have been characterised by static light scattering, with however little impact of the entrapped particle on the overall cluster structure.

External electric and magnetic fields have rather obviously been applied to guide particles into linear assemblies. Magnetic nanoparticles may carry considerable dipole moments and have been suspected of chain formation quite some time ago. [112-114] This was recently demonstrated by the Biswal group [115, 116] using micron-sized paramagnetic particles, which are linked with DNA molecules under magnetic field. Such a system, in analogy with the well-known bead-spring polymer model, forms linear chains of different flexibility depending on both the linker length and the inter-particle spacing controlled by the field strength. Still in the field of magnetic ordering, field-induced assemblies of nanoparticles have been investigated recently by small-angle scattering of polarized neutrons by Fu et al. [117] And Malik et al [118] have studied nanometric core-shell iron oxide ellipsoids and their assembly. In order to avoid capillarity effects during drying for electron microscopy, they perform SAXS in the presence of magnetic fields. Depending on the exact magnetic nature and the existence of a shielding silica layer on the NP surface, a more or less close-packed ordering of these NPs is observed, at least on small scales.

The dielectric force acting on particles in non-uniform electric fields scaling with the third power of the particle size, the attractive effect is stronger for bigger particles, and studies with electric fields focus mostly on micron-sized particles. Dielectric micro-particles have been assembled by Bharti et al. [78] The chains of identical particles break up in pieces upon switching off the AC field. The authors found that they can stabilise such chains by "gluing" them with smaller NPs of opposite charge. The formation of permanently bound polymeric particles brought together by an aligning electric field has been published by Vutukuri et al. [119] In this case, the chain stability once the field is switched off relies on a bonding step using short annealing at temperature below T_g. Two years later, again Barthi et al have further investigated the importance of the size ratio on the length of the structures, [120] and in 2015 they reviewed the assembly methods using field-induced interactions, including anisotropic and patchy particles [121]. The field-assisted assembly of the latter in crystalline structures has been reported by Song et al. [122] The formation of two-dimensional structures has been pioneered by Gangwal et al, [123] using an alternating electric field and patchy metallo-dielectric particles. Optical micrographs show the formation of chains parallel to the low-frequency field, and perpendicular structures at high frequencies. The formation of these unusual frequency-dependent assembly configurations could be explained by the change in polarisability of the polymer as opposed to metallic patches, resulting in superimposing dipoles and thus inducing multi-polar interactions, with components perpendicular to the field. The use of two guiding fields to form 2D assemblies has recently been published by Barthi et al, using a superposition of perpendicular electric and magnetic fields. [124] The authors rationalise their findings in terms of chain formation of nanoparticles, which then self-assemble into FCC supercrystals, the 2D-scattering pattern of which is easily identified. To conclude on the use of external electric fields to trigger specific particle assemblies, it may be noted that homogeneous particles follow the intuitive expectation and align parallel to a unique field, due to the interaction of induced dipoles. More complex particles may possess multipolar potentials, which may trigger aggregation in directions perpendicular (or some intermediate direction) to the external field, up to two-dimensional percolation processes. Adding a second field may also play that role. Once the fields are turned off, Brownian motion breaks up the chains, unless either capillary interaction such as between annealed polymer particles, or other, sticky particles are added to consolidate the bonds. It is unclear at the moment how these new building blocks can be positioned and used beyond simple percolation, but the first step of self-assembly has been made. The effects of electric or magnetic fields with or without modulation in space and time on particle self-assembly have been reviewed by van Blaaderen et al in 2013. [125] Although we are interested here in aggregates of particles in contact, two dimensional non close-packed arrays of colloidal particles with tunable interparticle distance may also be fabricated using more complex sequences of electric fields. They are stable after both field and solvent removal, with potential applications as lithographic masks, or templates for photonic crystals, as discussed by Gong and Wu. [126]

III.3 From aggregation to applications

Potentially useful nanoparticle properties are obviously linked to the small dimensions of NPs, or at least to one small dimension, as it is the case with clay platelets possessing a nanometric thickness. NPs may be small enough to make quantum effects measurable, in particular spectroscopically. Aggregating NPs brings surfaces in contact, and modifies or enhances spectroscopic responses characteristic of the NPs and molecules at their surface, opening the road to using aggregates for, e.g., molecular sensing. This and other applications will be discussed below, in the spirit of giving an overview. Secondly, nanoparticles are mostly used for one predominant property, high available surface area. The best possible dispersion is therefore often sought, but not always: NPs can be regrouped in space into aggregates, which still undergo Brownian motion collectively, and which can themselves be arranged using the full range of colloidal interactions, opening the road to higher hierarchical order. In this last part of this review article, we will emphasize a particular application of NP aggregation, making both use of high surface area and the formation of volume-spanning aggregates, polymer nanocomposites.

Before discussing aggregate formation in polymer nanocomposites, other prominent applications of nanoparticle aggregation may be mentioned. Among the oldest applications of colloidal structure formation was the use of ceramics dating back to the early days of homo sapiens, which however is way out of the time window we wish to review here. The interested reader is referred to a review article. [127] In more modern times, the influence of particle contact on plasmon resonance of metallic NPs has been used by many groups to detect aggregation, see for instance the aggregation of gold NPs around a biopolymer structure [128]. The observed colour changes may then be used to detect changes on a molecular level, e.g., play the role of colorimetric reporters in biosensors, as reviewed by Aldewachi et al [129] recently.

The optical properties of pigment nanoparticles suspended in water – i.e., inks – are intimately related to their dispersion, which may be transformed when the ink dries. Water is then replaced by matrix molecules, namely binders, and the resulting structural hierarchy of the pigment particles controls final product appearance, but also shelf life. Mulderig et al have looked into the development of structure of surfactant-stabilized NPs as a function of primary particle size recently. [130] They focus on the 2nd virial coefficient describing interactions between particles, an approach extended to nanocomposites below. Based on the unified Beaucage model for small-angle scattering,[36, 37] the experimental observation is a gradual shift with increasing primary particle size from stable aggregates of hundreds of small particles (diameter 8 nm, with a positive 2nd virial coefficient), to smaller aggregates of bigger particles, with lower fractal dimension, until very small aggregates of big particles (52 nm) are found. They rationalise their scattering data in terms of the interplay between short-range attractive interaction favouring the formation of aggregates for the smallest primary particles, with long-range

repulsion which stabilizes these aggregates. Repulsion becomes negligible for the big particles, and the authors identify the moment when its disappearance will ultimately induce phase separation.

Medical applications may also be mentioned. For example, the controlled aggregation of superparamagnetic iron NPs (SPIONS), which may find applications in signal enhancement for contrast agents in imaging, hyperthermia treatments, or targeted drug delivery, will be discussed below. A general review on the synthesis and use of aggregated magnetic NPs (called supraparticles) has been written by Guo et al. [131]

The fabrication and study of metamaterials has become an entire sub-discipline, the thourough review of which is outside our scope. As an example of controlled colloidal self-assembly leading to a magnetic nanostructure, in an approach similar to the generation of patchy particles by nanoparticle adsorption, the article by Gomez-Graña et al may be cited. [132] These authors fix the nanostructure by growing an additional silica layer on particles, and self-assemble them in random close packing on a higher hierarchical level, using a microfluidic evaporator. They thus obtain a macroscopic metamaterial, and demonstrate its properties using spectroscopic ellipsometry.

The main focus of applications in this review is on polymer nanocomposites (PNCs). These materials are made of nanoparticles embedded in a polymer matrix. The spatial arrangement of the nanoparticles, and in particular their aggregation, has a dominating influence on macroscopic properties of the material, including optical transparency,[133] dielectric constant, [134] or shear or elongational moduli,[135] with obvious relevance for applications like car tire threads. [136] The transmission of any quantity, be it electric current or momentum, from one particle to the next is obviously related to the NP dispersion, and small-angle scattering is well-suited to follow particle arrangements and re-arrangements, i.e. particle correlations, see for instance a recent review [137]. The process of nanocomposite formulation is crucial, but does usually not take place at thermodynamic equilibrium, e.g., due to the input of mechanical mixing energy in industrial systems. Nonetheless, the final aggregation state is strongly influenced by interaction free energies between NPs, as in all examples discussed up to here.

In the previous section, we have discussed the drying route of colloidal suspensions used by Moro et al [59] to reach a different final powder state, by modifying the structural evolution in water during drying. Here, we will discuss a variant of this approach used to formulate polymer nanocomposites, where the medium is changed by evaporating one of the suspending components, while another one – polymer molecules – forms a continuous matrix. In this case, a surface modification of the nanoparticles may change both the interactions in the first medium, and in the second, thereby allowing a control over the particle dispersion in nanocomposites.

One of the first quantitative examples of the formation of aggregates of controlled size in *model* polymer nanocomposites has been obtained by “freezing in” a destabilised aqueous NP dispersion. [138]

This allowed to show the correlation between the aggregation numbers measured by SANS with the mechanical response, see [138] and references therein, followed by more detailed studies, [139] in particular of chain mass governing viscosity and thus particle reorganisations [20]. While the latter approach [20] was based on a purely 'geometrical' measurement of aggregation from the combination of TEM and small-angle scattering, Lin et al [140] have recently attempted to extract thermodynamic potentials from a multi-scale aggregated structure of palladium-NPs in low-mass poly(2-vinylpyridine) (P2VP). By small-angle scattering, they have observed three different levels of structure, ranging from individual NPs forming small aggregates, which themselves cluster quite densely on larger scales, described by a fractal dimension of about 2.3. Their approach is based on a description of the scattering of finite-sized aggregates made of monodisperse spheres, polydispersity of particles and aggregates being accounted for via the average form factors of both. Through their quantitative modelling, Lin et al find that attractive interactions (sticky hard spheres) must be included in the treatment, the fits allowing a determination of the depth of the attractive tail of about 2 kT. They have then applied a similar description to a study of the same NPs formed by in-situ reduction, focusing on the time evolution of the SAXS intensity. [141] The particle volume fraction increases with time, allowing them to follow a specific kinetic pathway of aggregation, entering a two-phase region. It is interesting to note the presence of a correlation hole in some of their figures, which could now be used to determine local densities. The approach proposed by Lin et al is more complex and is again based on detailed modelling of each structure, in particular mass fractals.

Kim et al [142] have used SAXS to study the aggregate formation during drying of polymer nanocomposites, namely silica in poly(vinyl alcohol) (PVA). They used a special vertical scattering set-up at the synchrotron DESY (Hamburg, Germany), allowing them to follow filler structure during drying as a function of the physico-chemical parameters, in particular the pH governing interactions between polymer and NPs in suspension, as shown in Figure 6. At high pH, the charge-stabilised NPs gradually lose their stability, as can be concluded from the progressive shift of the peak position, whereas they immediately stick together at low pH, forming large-scale structures in suspension with a corresponding low-q upturn. Thus due to the different pH-dependence of electrostatic stabilisation, polymer adsorption, and depletion, different particle superstructures are formed at low and high pH, the best liquid dispersion being paradoxically transformed into the most aggregated nanocomposite structure due to depletion-induced aggregate formation. One may note that the choice of the casting solvent is also an important parameter to control the final dispersion state. [143]

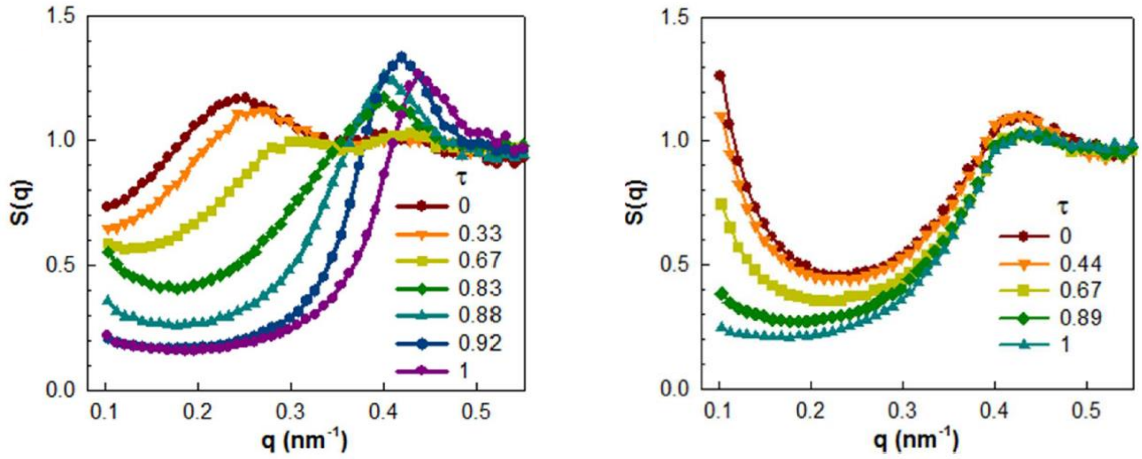

Figure 6: Structure factor as a function of drying time τ for silica-PVA suspensions at high **(left)** and low pH **(right)** by Kim et al. [142] Reproduced with permission from [142]. Copyright (2016) American Chemical Society.

In subsection III.1, we have discussed the effect of grafting small molecules on NPs in order to change their interactions with the surrounding matrix. We have recently used organosilanes of different grafting function but identical hydrophobicity in solvent-cast model systems to modify the polymer-particle interactions in styrene-butadiene (SB) systems filled with silica. [48] A newly developed simulation technique has been applied to the SAXS-data, based on a reverse Monte Carlo procedure producing a sequence of polydisperse particle dispersion states compatible with the scattering, and an aggregate recognition algorithm to find and analyse aggregates in these sequences. This allows determining average aggregation states, and follow them from the original suspension to nanocomposites, for each grafting function, as shown in Figure 7, where the intensity curves on the left are analysed in terms of aggregate mass distributions on the right-hand side. In the final SB matrix, trifunctional ethoxy-C_8 grafting is found to limit aggregation better than methoxy (C_{8m}), or even monomethoxy (C_{8mm}) functions. Besides electrostatic charges varying with grafting function, differences in interactions may be due to patch formation at the NP surface favoured by polycondensation of trifunctional as opposed to monofunctional molecules. It should be mentioned that much more ambitious reverse Monte Carlo simulations using massively parallelised code have been applied to scattering from nanocomposites made of silica dispersed in the crosslinked car-tire polymer material, styrene-butadiene rubber (SBR), recently. [144] This is an industrial system, but it is discussed here due to the proximity of the RMC approaches. Hagita et al [144] simulate enormous numbers of (monodisperse) NPs, typically 2^{25}, allowing them to reproduce the scattering data and to obtain real-space pictures comparable to experimental TEM. Interestingly, they find that the changes in dispersion induced by the use of end-functionalised polymer chains is reflected in the peak of the pair-correlation function, but that the global dispersion visible as voids in TEM and simulation is better recognised by identifying free volumes in a 3D topological analysis, based on Voronoi cells.

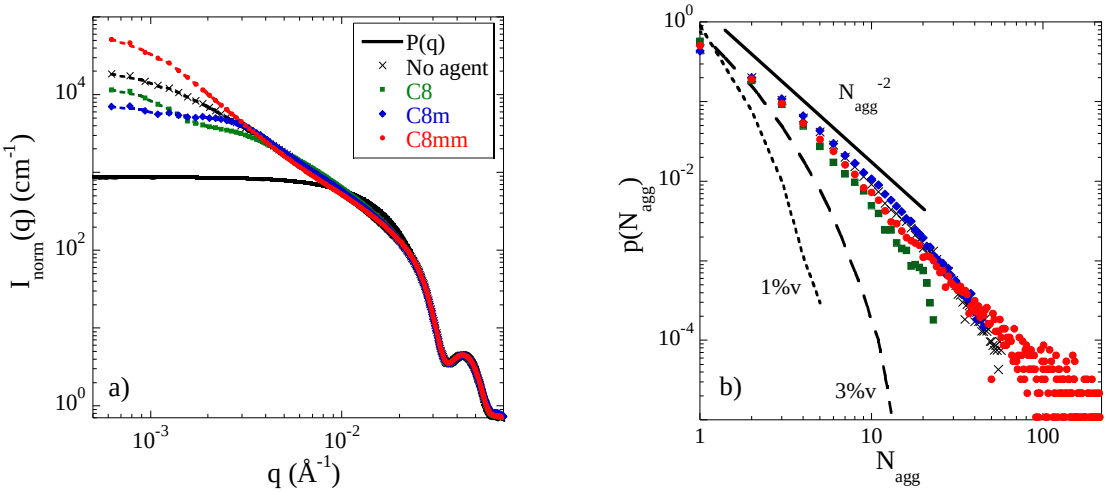

Figure 7: (a) Scattered SAXS intensity normed to NP form factor (P(q), R_0 = 12.5 nm, σ = 0.12) of polymer nanocomposites made with bare, and C_8-, C_{8m}-, and C_{8mm}-surface modified NPs, superimposed to reverse Monte Carlo fits. **(b)** Corresponding aggregate mass distribution functions, compared to random dispersions of the same NPs with excluded volume. Reproduced with permission from [48]. Copyright (2018) American Chemical Society.

Besides the commonly used organosilane molecules, phosphonic acids may be employed, in particular if the starting solvent is water, where silanes may polycondense. Water-borne latex nanocomposites reinforced with phosphonic acid-grafted alumina-silica NPs have been studied by Schmitt-Pauly et al using small-angle scattering and TEM. [145] While the overall aggregate size is outside the experimental window in scattering, the local particle density could be determined using the correlation hole analysis based on eq.(5), and followed as a function of type and density of the grafts. Interestingly, when comparing to the aqueous dispersion discussed above, the local structure is found to be reorganised in the hydrophobic matrix. This clearly indicates that the particles can rearrange even in the viscous polymer matrix. For completeness, the fate of TiO_2 nanoparticles grafted with phosphonic acids and incorporated in different polymers by solvent casting should also be mentioned. [146] In this case, the grafting density cannot be controlled, but depending on the type of graft, and its compatibility with the polymer matrix, more or less dense NP assemblies are created.

The next more complicated system is still a model system, i.e., made of well-defined NPs, but with short polymer molecules grafted on their surface. Heo et al [147] have studied the reversible aggregation of surface-modified gold nanoparticles using poly(styrene-r-2-vinylpyridine) (2.8 kg/mol) capable of hydrogen bonding with the polymer matrix, poly(styrene-r-4-vinyl phenol). Depending on the annealing temperature, the strength of H-bonding is weakened, and particles can reorganise in the relatively low molecular weight matrix (24 kg/mol) ensuring high mobility. TEM pictures as shown in Figure 8 provide evidence for different aggregation states with temperature, which the authors quantify by UV-vis spectroscopy, taking advantage of the shift in surface plasmon resonance with aggregation. In particular, a heating-cooling cycle evidences reversibility, at least at low NP volume

fractions. In a control experiment with polystyrene, which is insensitive to H-bonding, only aggregation is observed, without redispersion (see Figure 8).

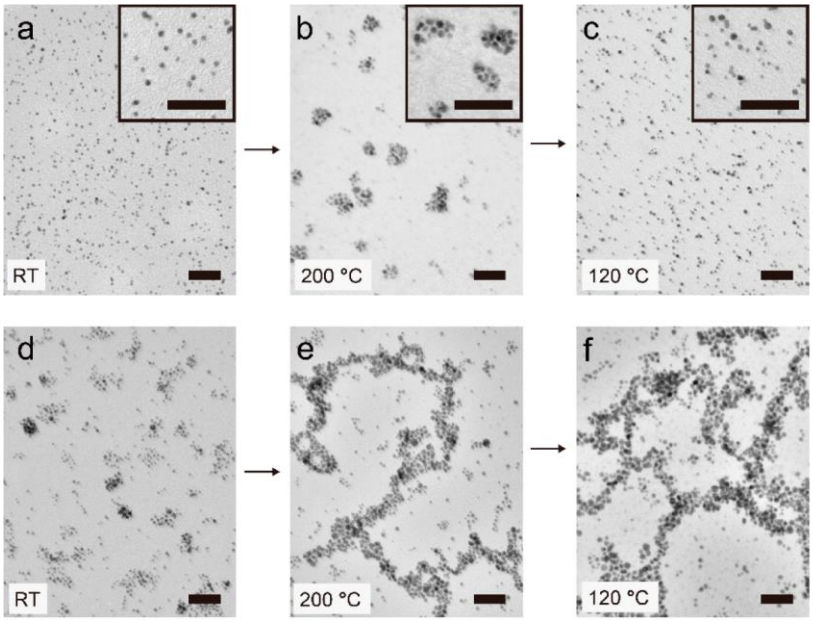

Figure 8: TEM images of nanocomposite films at different moments of the heating-cooling cycle from left to right. Top row: with H-bonding, bottom: control experiment without H-bonding. Reproduced with permission from [147]. Copyright (2013) American Chemical Society.

Polymer-grafted systems have been shown to be quite versatile, creating aggregated structures as a function of grafting density, and mass ratio between grafted and matrix chains. [148] The effect of the grafted layer is directly related to the physics of the polymer brushes, i.e., entropic effects, as illustrated recently by Qi et al [149] by adding temperature to the experimental parameter space. By varying the type of graft, as well as the grafting density, they show using several direct imaging methods the evolution from homogeneous dispersions to clustering.

Zhao et al [150] have extended the study of the influence of the type of grafted layers on nanocomposite structure by using bidisperse layers. These layers are made of randomly mixed densely grafted short P2VP chains, and longer and sparser PS chains, all dispersed in PS matrices of various masses. The authors find that due to the existence of the thin and dense P2VP-layer, the strong attraction between NPs is suppressed, favouring generally better dispersion. The long chains, however, still reproduce key features of their respective monolayers, in particular the formation of anisotropic aggregates, like strings, sheets, and connected superstructures. Note that the same group has also compared the morphologies of nanocomposites made with NPs carrying such bidisperse brushes to particles modified by block copolymer adsorption, the latter favouring dispersion. [151]

It seems at first sight rather surprising to encounter such a large variety of structures in polymer nanocomposites made with grafted NPs, just like with the endless possibilities of combining patchy

nanoparticles as described in subsection III.2. Asai et al [152] have recently shown that lightly grafted nanoparticles can be looked at as Janus particles, thus favouring the formation of similar structures. Moreover, these authors draw an analogy with geometrical constructions as in surfactant science ("packing parameter"), allowing to rationalise the formation of anisotropic aggregates. Indeed, as already mentioned, polymer-covered nanoparticles have been made patchy using a thermodynamically driven segregation of the polymer layer in solvent by Choueiri et al. [103]

To finish this paragraph about model systems, the currently most successful approach to perfect dispersion should also be mentioned. In a recent study, Feld et al [153] have made perfect use of SAXS and TEM to show that superparamagnetic iron oxide NPs (SPION) could be encapsulated in an ultimately crosslinked diblock copolymer before redispersion in PEO by phase transfer. Similar NPs have also been aggregated in a controlled manner by Hajduova et al [154] and Wozniak et al [155] using the double-hydrophilic copolymer popularised by Berret.

Model systems formulated with calibrated and well-dispersed nanoparticles are crucial for understanding nanocomposite physics. This starts with structural characterisation, which for both scattering and electron microscopy is far easier with nice spheres than with disordered lumps of filler. It is nonetheless important to make progress also on nanocomposites of industrial relevance, which are usually made by solid-phase mixing of dry particle powders with polymer. The resulting structure provides considerable improvement of, e.g., mechanical properties, but due to the polydisperse nature of the particles, it is difficult to apprehend it quantitatively. Therefore, studies have concentrated for a long time on try-and-error formulations, varying the many industrial ingredients, and studying the macroscopic response only. At most, electron microscopy was compatible with some aggregation picture, which however was mainly drawn from formulation history and rheological measurements, with the notable exception of studies of the filler alone. [156, 157] To our best knowledge, the first group proposing a concept to the interpretation of small-angle scattering data was Japanese, in an article by Shinohara et al. [158] They convincingly assigned the different scattering regimes of industrial nanocomposites to a hierarchical structure of polydisperse NPs, aggregates, and clusters of aggregates. We have then proposed a quantitative model of the microstructure of simplified industrial nanocomposites. [6] Here 'simplified' refers to the reduction of ingredients, and the use of well-defined uncrosslinked SB polymer chains, whereas the filler was truly industrial. Our model is based on the correlation hole approach formulated for aggregates, see section I, and it allows to estimate the average size and mass of aggregates. It has then been applied to variations of grafting density of the polymer, [159] chain mass, [160, 161] and the entire study has been summarized in a review [162]. The underlying structure of all these samples is a large-scale organisation in sheets or branches filled with aggregates of some 50 NPs, at internal densities κ of ca. 35%, leading to a typical aggregate radius of some 45 nm, details depending on the exact composition. In particular, the rheological response of the material could be described using a simple model of aggregate percolation, using κ of the aggregates

determined by scattering. The model has also been applied by Musino et al [163] to investigate the influence of small molecules, namely an amine catalyser and an organosilane (C_8), both commonly used in industrial applications, on the final aggregate structure. It was found that the combination of both molecules induces the strongest decrease in aggregate mass, i.e., the best dispersion, a result most likely empirically known by formulation managers in the tire industry. [163] Very recently, a much more complete theoretical treatment following the same idea as Baeza et al [6] has been applied by Yamaguchi et al [164] to closely related samples, including again end-graftable chains.

As fractality is one of the simplest ordering principles of apparently disordered matter, and small-angle scattering picks up fractal dimensions easily, it is no wonder that many research groups have applied eq.(4) to polymer nanocomposites of industrial relevance. In its unified form proposed by Beaucage, [36, 165] it can be applied to multi-level structures, of different fractal dimension, and a finite size can be attributed via a Guinier expression to each level, see for instance [166, 167]. Recently, a pseudo-thermodynamic analysis has been proposed by Jin et al, [168] based on the second virial coefficient expressing particle or aggregate interactions, see also [130] for the 'real' thermodynamic analysis. Here 'pseudo' refers to the fact that mechanical driving forces to dispersion are treated in analogy to thermal ones, leading empirically to the same observation of dispersion by scattering. The virial coefficient is combined with a unified fractal law description of scattering via a random phase approximation approach. As a result, the concentration-dependent interactions between aggregates induce a decrease of the intermediate-q intensity, closely resembling the first analyses by Shinohara [158] or Baeza [6], relating such a decrease to the improvement of the dispersion in the polymer matrix. It currently looks like the mean-field thermodynamic approach by Beaucage is best suited for carbon black nanoparticles and suspended pigments, whereas silica shows specific correlations better captured by a colloidal structure factor approach.

IV. Conclusions and outlook

Recent progress in the control of aggregation of nanoparticles has been reviewed, attempting to follow the development of increasingly complex interactions designed to provide specific aggregation properties. We have concentrated our efforts on particle self-assembly in three dimensions – in suspension or matrices –, and described only occasionally clusters of lower dimensionality. The experimental determination of aggregate morphology or structure, namely by scattering techniques and electron microscopy, is another point which we have highlighted throughout this review. Applications, finally, have been discussed in section III.3, with a special focus on polymer nanocomposites. One may hope that much more complex systems than model systems with NPs of well-defined size and shape will be studied with a sensibility for soft matter physics and chemistry, like for instance the particular impact of aggregated nanoparticles in environmental studies,[169] or the role of aggregates in digestion, see for example [170]. In any event, the study of such systems will be

highly interdisciplinary, as it is already the case for much of the research presented here, needing combined expertise from physics, chemistry, and biology. Contributions and mutual fertilisation from simulations, theory, and sophisticated experimental techniques will be ever more important in the future.

It has been understood a long time ago why aggregation sets in, and knowledge and mastering of interparticle interactions have allowed rather precise control of local correlations, bonding, and resulting aggregate shapes and sizes. However, the most common case is still that aggregation is controlled in the sense that the fractal dimension of resulting clusters can be tuned, and more rarely also the overall size, possibly by kinetic factors. Patchy colloids use the advantage of directional interactions to build well-defined self-assembled structures. These are promising systems, where scalability is now the main challenge to overcome. Clearly, the magic combination of producing large quantities (i.e., closer to the Avogadro number than to unity) of well-defined objects is still a primary objective of current day research, and this will probably stay this way in the foreseeable future.

Conflicts of interest: There are no conflicts of interest to declare.

Acknowledgements: We thank Soft Matter for inviting, motivating, and finally waiting patiently for this review article. The authors are grateful for support by the ANR NANODYN project, grant ANR-14-CE22-0001-01 of the French Agence Nationale de la Recherche. Finally, progress in the understanding of colloidal structures benefits greatly from small-angle scattering beamtimes granted by large-scale facilities, in particular ESRF (Grenoble), Soleil (St Aubin), LLB (Saclay), ILL (Grenoble), and MLZ (München).

References

1 S. Horikoshi and N. Serpone, in *Microwaves in Nanoparticle Synthesis*, Wiley-VCH Verlag GmbH & Co. KGaA, 2013, pp. 1-24.

2 M. Benelmekki, in *Designing Hybrid Nanoparticles*, Morgan & Claypool Publishers, 2015, pp. 1-1-1-14.

3 J. N. Israelachvili, in *Intermolecular and Surface Forces (Third Edition)*, Academic Press, San Diego, 2011.

4 W. B. Russel, D. A. Saville and W. R. Schowalter, *Colloidal Dispersions*, Cambridge University Press, Cambridge, 1989.

5 P. Lindner, *Neutrons, X-ray and Light Scattering*, North Holland, Elsevier, 2002.

6 G. P. Baeza, A. C. Genix, C. Degrandcourt, L. Petitjean, J. Gummel, M. Couty and J. Oberdisse, *Macromolecules*, 2013, **46**, 317-329.

7 A. Dorigato, Y. Dzenis and A. Pegoretti, *Mechanics of Materials*, 2013, **61**, 79-90.

8 T. A. Witten, M. Rubinstein and R. H. Colby, *J Phys II*, 1993, **3**, 367-383.
9 B. Schroyen, J. W. Swan, P. Van Puyvelde and J. Vermant, *Soft Matter*, 2017, **13**, 7897-7906.
10 W. Yu, J. Wang and W. You, *Polymer*, 2016, **98**, 190-200.
11 S. K. Kumar, B. C. Benicewicz, R. A. Vaia and K. I. Winey, *Macromolecules*, 2017, **50**, 714-731.
12 C. Wang, F. C. Cheong, D. B. Ruffner, X. Zhong, M. D. Ward and D. G. Grier, *Soft Matter*, 2016, **12**, 8774-8780.
13 A. Mohraz and M. J. Solomon, *Langmuir*, 2005, **21**, 5298-5306.
14 S. Ahn and S. J. Lee, *Soft Matter*, 2014, **10**, 3897-3905.
15 F. Dalmas and L. Roiban, in *Functional and Physical Properties of Polymer Nanocomposites*, John Wiley & Sons, Ltd, 2016, pp. 7-27.
16 L. Song, Z. Wang, X. Tang, L. Chen, P. Chen, Q. Yuan and L. Li, *Macromolecules*, 2017, **50**, 7249-7257.
17 F. Dalmas, N. Genevaz, M. Roth, J. Jestin and E. Leroy, *Macromolecules*, 2014, **47**, 2044-2051.
18 B. A. Legg, M. Zhu, L. R. Comolli, B. Gilbert and J. F. Banfield, *Langmuir*, 2014, **30**, 9931-9940.
19 C. R. Murthy, B. Gao, A. R. Tao and G. Arya, *Nanoscale*, 2015, **7**, 9793-9805.
20 A. Banc, A. C. Genix, M. Chirat, C. Dupas, S. Caillol, M. Sztucki and J. Oberdisse, *Macromolecules*, 2014, **47**, 3219–3230.
21 N. Jouault, F. Dalmas, F. Boué and J. Jestin, *Polymer*, 2014, **55**, 2523-2534.
22 H. Häbel, A. Särkkä, M. Rudemo, C. Hamngren Blomqvist, E. Olsson, C. Abrahamsson and M. Nordin, *Journal of Microscopy*, 2016, **262**, 102-111.
23 https://www.neutron-sciences.org/component/issues/.
24 L. A. Feigin and D. I. Svergun, *Structure analysis by small-angle X-ray and neutron scattering*, Plenum Press, New York, 1987.
25 J. P. Hansen and I. R. McDonald, *Theory of Simple Liquids*, Academic Press, London, 1986.
26 K. Hiroike, *Journal of the Physical Society of Japan*, 1969, **27**, 1415-&.
27 J. K. Percus and G. J. Yevick, *Physical Review*, 1958, **110**, 1-13.
28 J. B. Hayter and J. Penfold, *Molecular Physics*, 1981, **42**, 109-118.
29 J.-P. Hansen and J. B. Hayter, *Molecular Physics*, 1982, **46**, 651-656.
30 R. J. Baxter, *J. Chem. Phys.*, 1968, **49**, 2770-2774.
31 J. Oberdisse, P. Hine and W. Pyckhout-Hintzen, *Soft Matter*, 2007, **2**, 476-485.
32 J. K. Kjems, T. Freltoft, D. Richter and S. K. Sinha, *Physica B+C*, 1986, **136**, 285-290.
33 S. K. Sinha, *Physica D: Nonlinear Phenomena*, 1989, **38**, 310-314.
34 P. Meakin, *Journal of Sol-Gel Science and Technology*, 1999, **15**, 97-117.
35 J. Teixeira, *Journal of Applied Crystallography*, 1988, **21**, 781-785.
36 G. Beaucage, *J. Appl. Cryst.*, 1995, **28**, 717-728.

37 G. Beaucage, T. A. Ulibarri, E. P. Black and D. W. Schaefer, *Hybrid Organic-Inorganic Composites*, 1995, **585**, 97-111.

38 *Procedings of the NATO Advanced Study Institute on Novel approaches to the structure and dynamics of liquids : experiments, theories and simulations*, Springer 2004.

39 B. Chu, Y. Li and T. Gao, *Review of Scientific Instruments*, 1992, **63**, 4128-4133.

40 D. W. Schaefer and M. M. Agamalian, *Current Opinion in Solid State and Materials Science*, 2004, **8**, 39-47.

41 S. Desert, V. Thevenot, J. Oberdisse and A. Brulet, *J. Appl. Cryst.*, 2007, **40**, s471-477.

42 J. Lambard, P. Lesieur and T. Zemb, *J. Phys. I France*, 1992, **2**, 1191-1213.

43 F. Zhang and J. Ilavsky, *Polymer Reviews*, 2010, **50**, 59-90.

44 P. Lindner, R. P. May and P. A. Timmins, *Physica B: Condensed Matter*, 1992, **180-181**, 967-972.

45 M. Sztucki and T. Narayanan, *Journal of Applied Crystallography*, 2007, **40**, s459-s462.

46 L. de Martín, W. G. Bouwman and J. R. van Ommen, *Langmuir*, 2014, **30**, 12696-12702.

47 A.-C. Genix and J. Oberdisse, *Soft Matter*, 2017, **13**, 8144-8155.

48 D. Musino, A. C. Genix, T. Chaussée, L. Guy, N. Meissner, R. Kozak, T. Bizien and J. Oberdisse, *Langmuir*, 2018, **34**, 3010–3020.

49 P. Müller-Buschbaum, in *Applications of Synchrotron Light to Scattering and Diffraction in Materials and Life Sciences*, eds. M. Gomez, A. Nogales, M. C. Garcia-Gutierrez and T. A. Ezquerra, Springer Berlin Heidelberg, Berlin, Heidelberg, 2009, pp. 61-89.

50 Y. Le Diagon, S. Mallarino and C. Fretigny, *European Physical Journal E*, 2007, **22**, 77-83.

51 O. V. Tomchuk, D. S. Volkov, L. A. Bulavin, A. V. Rogachev, M. A. Proskurnin, M. V. Korobov and M. V. Avdeev, *The Journal of Physical Chemistry C*, 2015, **119**, 794-802.

52 S. Abbas, I. Yadav, S. Kumar, V. K. Aswal and J. Kohlbrecher, *Chemical Physics Letters*, 2017, **675**, 124-130.

53 H. Zhang, W. Wang, M. Akinc, S. Mallapragada, A. Travesset and D. Vaknin, *Nanoscale*, 2017, **9**, 8710-8715.

54 S. Saeki, N. Kuwahara, M. Nakata and M. Kaneko, *Polymer*, 1976, **17**, 685-689.

55 D. Babayan, C. Chassenieux, F. Lafuma, L. Ventelon and J. Hernandez, *Langmuir*, 2010, **26**, 2279-2287.

56 S. Kumar, V. K. Aswal and J. Kohlbrecher, *Langmuir*, 2012, **28**, 9288-9297.

57 G. Despert and J. Oberdisse, *Langmuir*, 2003, **19**, 7604-7610.

58 D. Lugo, J. Oberdisse, A. Lapp and G. Findenegg, *J Phys Chem B*, 2010, **114**, 4183-4191.

59 S. Moro, C. Parneix, B. Cabane, N. Sanson and J.-B. d'Espinose de Lacaillerie, *Langmuir*, 2017, **33**, 4709-4719.

60 H. Tigger-Zaborov and G. Maayan, *Journal of Colloid and Interface Science*, 2017, **508**, 56-64.

61 C. Schmitt Pauly, A.-C. Genix, J. G. Alauzun, M. Sztucki, J. Oberdisse and P. H. Mutin, *Phys. Chem. Chem. Phys.*, 2015, **17**, 19173-19182.

62 C. S. Pauly, A. C. Genix, J. G. Alauzun, G. Guerrero, M. S. Appavou, J. Perez, J. Oberdisse and P. H. Mutin, *Langmuir*, 2015, **31**, 10966-10974.

63 J. F. A. de Oliveira and M. B. Cardoso, *Langmuir*, 2014, **30**, 4879-4886.

64 W. Jiang, D. B. Hibbert, G. Moran, J. Herrmann, A. K. Jamting and V. A. Coleman, *Rsc Advances*, 2013, **3**, 7367-7374.

65 I. Izquierdo-Lorenzo, J. Kubackova, D. Manchon, A. Mosset, E. Cottancin and S. Sanchez-Cortes, *The Journal of Physical Chemistry C*, 2013, **117**, 16203-16212.

66 D. Ray, V. K. Aswal and J. Kohlbrecher, *Journal of Applied Physics*, 2015, **117**, 164310.

67 J. Meissner, A. Prause, B. Bharti and G. H. Findenegg, *Colloid Polym. Sci.*, 2015, **293**, 3381-3391.

68 I. Yadav, S. Kumar, V. K. Aswal and J. Kohlbrecher, *Physical Review E*, 2014, **89**, 032304.

69 I. Yadav, S. Kumar, V. K. Aswal and J. Kohlbrecher, *Langmuir*, 2017, **33**, 1227-1238.

70 B. Bharti, J. Meissner, S. H. L. Klapp and G. H. Findenegg, *Soft Matter*, 2014, **10**, 718-728.

71 S. Mehan, V. K. Aswal and J. Kohlbrecher, *Langmuir*, 2014, **30**, 9941-9950.

72 S. Kumar, V. K. Aswal and J. Kohlbrecher, *Langmuir*, 2016, **32**, 1450-1459.

73 S. Kumar, D. Ray, V. K. Aswal and J. Kohlbrecher, *Physical Review E*, 2014, **90**, 042316.

74 F. Li, D. Sun, T. Wu and Y. Li, *Soft Matter*, 2017, **13**, 1539-1547.

75 L. Shi, F. Carn, F. Boue, G. Mosser and E. Buhler, *Soft Matter*, 2013, **9**, 5004-5015.

76 A. M. Kalsin, M. Fialkowski, M. Paszewski, S. K. Smoukov, K. J. M. Bishop and B. A. Grzybowski, *Science*, 2006, **312**, 420-424.

77 W. Lin, M. Kobayashi, M. Skarba, C. Mu, P. Galletto and M. Borkovec, *Langmuir*, 2006, **22**, 1038-1047.

78 B. Bharti, G. H. Findenegg and O. D. Velev, *Scientific Reports*, 2012, **2**, 1004.

79 C. Zeng, Y. Chen, K. Kirschbaum, K. J. Lambright and R. Jin, *Science*, 2016, **354**, 1580-1584.

80 J. F. Berret, *Advances in Colloid and Interface Science*, 2011, **167**, 38-48.

81 J. P. Chapel and J. F. Berret, *Current Opinion in Colloid & Interface Science*, 2012, **17**, 97-105.

82 H.-J. Jang and H.-Y. Lee, *Colloids and Surfaces A: Physicochemical and Engineering Aspects*, 2018, **538**, 574-582.

83 Y. Nakamura, M. Okachi, A. Toyotama, T. Okuzono and J. Yamanaka, *Langmuir*, 2015, **31**, 13303-13311.

84 I. C. Gârlea, E. Bianchi, B. Capone, L. Rovigatti and C. N. Likos, *Current Opinion in Colloid & Interface Science*, 2017, **30**, 1-7.

85 E. Bianchi, B. Capone, I. Coluzza, L. Rovigatti and P. D. J. van Oostrum, *Physical Chemistry Chemical Physics*, 2017, **19**, 19847-19868.

86 Z. Zeravcic, V. N. Manoharan and M. P. Brenner, *Proceedings of the National Academy of Sciences*, 2014, **111**, 15918-15923.

87 É. Duguet, C. Hubert, C. Chomette, A. Perro and S. Ravaine, *Comptes Rendus Chimie*, 2016, **19**, 173-182.

88 S. Ravaine and E. Duguet, *Current Opinion in Colloid & Interface Science*, 2017, **30**, 45-53.

89 T. S. Skelhon, Y. Chen and S. A. F. Bon, *Soft Matter*, 2014, **10**, 7730-7735.

90 M. Sabapathy, Y. Shelke, M. G. Basavaraj and E. Mani, *Soft Matter*, 2016, **12**, 5950-5958.

91 T. A. Gschneidtner, Y. A. D. Fernandez, S. Syrenova, F. Westerlund, C. Langhammer and K. Moth-Poulsen, *Langmuir*, 2014, **30**, 3041-3050.

92 A. Klinkova, H. Thérien-Aubin, R. M. Choueiri, M. Rubinstein and E. Kumacheva, *PNAS*, 2013, **110**, 18775-18779.

93 R. M. Choueiri, E. Galati, A. Klinkova, H. Therien-Aubin and E. Kumacheva, *Faraday Discussions*, 2016, **191**, 189-204.

94 R. Schreiber, I. Santiago, A. Ardavan and A. J. Turberfield, *ACS Nano*, 2016, **10**, 7303-7306.

95 I. A. Trantakis, S. Bolisetty, R. Mezzenga and S. J. Sturla, *Langmuir*, 2013, **29**, 10824-10830.

96 N. C. M. and A. Michael, *Angewandte Chemie International Edition*, 2002, **41**, 3779-3783.

97 W. B. Rogers, W. M. Shih and V. N. Manoharan, *Nature Reviews Materials*, 2016, **1**, 16008.

98 F. Lu, K. G. Yager, Y. Zhang, H. Xin and O. Gang, *Nature Communications*, 2015, **6**, 6912.

99 Y. Wang, Y. Wang, D. R. Breed, V. N. Manoharan, L. Feng, A. D. Hollingsworth, M. Weck and D. J. Pine, *Nature*, 2012, **491**, 51.

100 Z. Xiaolong, L. Mingzhu, H. Mingxin, P. D. J. and W. Marcus, *Angewandte Chemie*, 2017, **129**, 5599-5603.

101 A. Désert, C. Hubert, Z. Fu, L. Moulet, J. Majimel, P. Barboteau, A. Thill, M. Lansalot, E. Bourgeat-Lami, E. Duguet and S. Ravaine, *Angewandte Chemie International Edition*, 2013, **52**, 11068-11072.

102 Y. Wang, Y. Wang, X. Zheng, G.-R. Yi, S. Sacanna, D. J. Pine and M. Weck, *Journal of the American Chemical Society*, 2014, **136**, 6866-6869.

103 R. M. Choueiri, E. Galati, H. Thérien-Aubin, A. Klinkova, E. M. Larin, A. Querejeta-Fernández, L. Han, H. L. Xin, O. Gang, E. B. Zhulina, M. Rubinstein and E. Kumacheva, *Nature*, 2016, **538**, 79.

104 S. Ni, J. Leemann, I. Buttinoni, L. Isa and H. Wolf, *Science Advances*, 2016, **2**.

105 S. Ni, H. Wolf and L. Isa, *Langmuir*, 2018.

106 C. Hamon, S. Novikov, L. Scarabelli, L. Basabe-Desmonts and L. M. Liz-Marzán, *ACS Nano*, 2014, **8**, 10694-10703.

107 M. Grzelczak, J. Vermant, E. M. Furst and L. M. Liz-Marzán, *ACS Nano*, 2010, **4**, 3591-3605.

108 A. P. R. Eberle and L. Porcar, *Current Opinion in Colloid & Interface Science*, 2012, **17**, 33-43.

109 D. P. Kalman and N. J. Wagner, *Rheologica Acta*, 2009, **48**, 897-908.

110 A. P. R. Eberle, N. Martys, L. Porcar, S. R. Kline, W. L. George, J. M. Kim, P. D. Butler and N. J. Wagner, *Physical Review E*, 2014, **89**, 050302.

111 X. Meng, H. Wu and M. Morbidelli, *Soft Matter*, 2016, **12**, 3696-3702.

112 E. Dubois, R. Perzynski, F. Boué and V. Cabuil, *Langmuir*, 2000, **16**, 5617-5625.

113 F. Gazeau, E. Dubois, J. C. Bacri, F. Boué, A. Cebers and R. Perzynski, *Physical Review E*, 2002, **65**, 031403.

114 M. Bonini, E. Fratini and P. Baglioni, *Materials Science and Engineering: C*, 2007, **27**, 1377-1381.

115 D. Li, J. Rogers and S. L. Biswal, *Langmuir*, 2009, **25**, 8944-8950.

116 J. Byrom, P. Han, M. Savory and S. L. Biswal, *Langmuir*, 2014, **30**, 9045-9052.

117 Z. Fu, Y. Xiao, A. Feoktystov, V. Pipich, M.-S. Appavou, Y. Su, E. Feng, W. Jin and T. Bruckel, *Nanoscale*, 2016, **8**, 18541-18550.

118 V. Malik, A. Pal, O. Pravaz, J. J. Crassous, S. Granville, B. Grobety, A. M. Hirt, H. Dietsch and P. Schurtenberger, *Nanoscale*, 2017, **9**, 14405-14413.

119 V. H. Rao, D. A. Faik, P. Bo, v. O. P. D. J., I. Arnout and v. B. Alfons, *Angewandte Chemie International Edition*, 2012, **51**, 11249-11253.

120 B. Bharti, G. H. Findenegg and O. D. Velev, *Langmuir*, 2014, **30**, 6577-6587.

121 B. Bharti and O. D. Velev, *Langmuir*, 2015, **31**, 7897-7908.

122 P. Song, Y. Wang, Y. Wang, A. D. Hollingsworth, M. Weck, D. J. Pine and M. D. Ward, *Journal of the American Chemical Society*, 2015, **137**, 3069-3075.

123 S. Gangwal, A. Pawar, I. Kretzschmar and O. D. Velev, *Soft Matter*, 2010, **6**, 1413-1418.

124 B. Bharti, F. Kogler, C. K. Hall, S. H. L. Klapp and O. D. Velev, *Soft Matter*, 2016, **12**, 7747-7758.

125 A. van Blaaderen, M. Dijkstra, R. van Roij, A. Imhof, M. Kamp, B. W. Kwaadgras, T. Vissers and B. Liu, *The European Physical Journal Special Topics*, 2013, **222**, 2895-2909.

126 J. Gong and N. Wu, *Langmuir*, 2017, **33**, 5769-5776.

127 G. V. Franks, C. Tallon, A. R. Studart, M. L. Sesso and S. Leo, *Journal of the American Ceramic Society*, 2017, **100**, 458-490.

128 D. K. Bozanic, A. S. Luyt, L. V. Trandafilovic and V. Djokovic, *Rsc Advances*, 2013, **3**, 8705-8713.

129 H. Aldewachi, T. Chalati, M. N. Woodroofe, N. Bricklebank, B. Sharrack and P. Gardiner, *Nanoscale*, 2018, **10**, 18-33.

130 A. Mulderig, G. Beaucage, K. Vogtt, H. Jiang, Y. Jin, L. Clapp and D. C. Henderson, *Langmuir*, 2017, **33**, 14029-14037.

131 J. Guo, W. Yang and C. Wang, *Advanced Materials*, 2013, **25**, 5196-5214.

132 S. Gomez-Grana, A. Le Beulze, M. Treguer-Delapierre, S. Mornet, E. Duguet, E. Grana, E. Cloutet, G. Hadziioannou, J. Leng, J. B. Salmon, V. G. Kravets, A. N. Grigorenko, N. A.

Peyyety, V. Ponsinet, P. Richetti, A. Baron, D. Torrent and P. Barois, *Materials Horizons*, 2016, **3**, 596-601.

133 S. Ehlert, C. Stegelmeier, D. Pirner and S. Förster, *Macromolecules*, 2015, **48**, 5323-5327.

134 K. Suematsu, M. Arimura, N. Uchiyama and S. Saita, *ACS Applied Nano Materials*, 2018.

135 J. Jancar, J. F. Douglas, F. W. Starr, S. K. Kumar, P. Cassagnau, A. J. Lesser, S. S. Sternstein and M. J. Buehler, *Polymer*, 2010, **51**, 3321-3343.

136 *The Science and Technology of Rubber (Fourth Edition)*, Academic Press, Boston, 2013.

137 A.-C. Genix and J. Oberdisse, *Current Opinion in Colloid & Interface Science*, 2015, **20**, 293-303.

138 J. Oberdisse, *Soft Matter*, 2006, **2**, 29-36.

139 M. Tatou, A. C. Genix, A. Imaz, J. Forcada, A. Banc, R. Schweins, I. Grillo and J. Oberdisse, *Macromolecules*, 2011, **44**, 9029-9039.

140 Y.-C. Lin, C.-Y. Chen, H.-L. Chen, T. Hashimoto, S.-A. Chen and Y.-C. Li, *The Journal of chemical physics*, 2015, **142**, 214905.

141 Y.-C. Lin, H.-L. Chen, T. Hashimoto and S.-A. Chen, *Macromolecules*, 2016, **49**, 7535-7550.

142 S. Kim, K. Hyun, B. Struth, K. H. Ahn and C. Clasen, *Macromolecules*, 2016, **49**, 9068-9079.

143 N. Jouault, D. Zhao and S. K. Kumar, *Macromolecules*, 2014, **47**, 5246-5255.

144 K. Hagita, T. Tominaga and T. Sone, *Polymer*, 2018, **135**, 219-229.

145 C. Schmitt Pauly, A.-C. Genix, J. G. Alauzun, J. Jestin, M. Sztucki, P. H. Mutin and J. Oberdisse, *Polymer*, 2016, **97**, 138-146.

146 A.-C. Genix, C. Schmitt-Pauly, J. G. Alauzun, T. Bizien, P. H. Mutin and J. Oberdisse, *Macromolecules*, 2017, **50**, 7721-7729.

147 K. Heo, C. Miesch, T. Emrick and R. C. Hayward, *Nano Letters*, 2013, **13**, 5297-5302.

148 S. K. Kumar, N. Jouault, B. Benicewicz and T. Neely, *Macromolecules*, 2013, **46**, 3199-3214.

149 D. Qi, F. Gao, Z. Chen, Z. Cui, G. Wang, N. Wang, Y. Zhang, G. Qu and Z. Cao, *Colloids and Surfaces A: Physicochemical and Engineering Aspects*, 2017, **523**, 106-117.

150 D. Zhao, M. Di Nicola, M. M. Khani, J. Jestin, B. C. Benicewicz and S. K. Kumar, *ACS Macro Letters*, 2016, **5**, 790-795.

151 D. Zhao, M. Di Nicola, M. M. Khani, J. Jestin, B. C. Benicewicz and S. K. Kumar, *Soft Matter*, 2016, **12**, 7241-7247.

152 M. Asai, A. Cacciuto and S. K. Kumar, *Soft Matter*, 2015, **11**, 793-797.

153 A. Feld, R. Koll, L. S. Fruhner, M. Krutyeva, W. Pyckhout-Hintzen, C. Weiß, H. Heller, A. Weimer, C. Schmidtke, M.-S. Appavou, E. Kentzinger, J. Allgaier and H. Weller, *ACS Nano*, 2017, **11**, 3767-3775.

154 J. Hajduová, M. Uchman, I. Šafařík, M. Šafaříková, M. Šlouf, S. Pispas and M. Štěpánek, *Colloids and Surfaces A: Physicochemical and Engineering Aspects*, 2015, **483**, 1-7.

155 E. Woźniak, M. Špírková, M. Šlouf, V. M. Garamus, M. Šafaříková, I. Šafařík and M. Štěpánek, *Colloids and Surfaces A: Physicochemical and Engineering Aspects*, 2017, **514**, 32-37.

156 D. W. Schaefer, T. Rieker, M. Agamalian, J. S. Lin, D. Fischer, S. Sukumaran, C. Chen, G. Beaucage, C. Herd and J. Ivie, *Journal of Applied Crystallography*, 2000, **33**, 587-591.

157 H. K. Kammler, G. Beaucage, D. J. Kohls, N. Agashe and J. Ilavsky, *Journal of Applied Physics*, 2005, **97**, 054309.

158 Y. Shinohara, H. Kishimoto, N. Yagi and Y. Amemiya, *Macromolecules*, 2010, **43**, 9480-9487.

159 G. P. Baeza, A. C. Genix, C. Degrandcourt, L. Petitjean, J. Gummel, R. Schweins, M. Couty and J. Oberdisse, *Macromolecules*, 2013, **46**, 6388–6394.

160 G. P. Baeza, A. C. Genix, C. Degrandcourt, J. Gummel, M. Couty and J. Oberdisse, *Soft Matter*, 2014, **10**, 6686–6695.

161 G. P. Baeza, A. C. Genix, C. Degrandcourt, J. Gummel, A. Mujtaba, K. Saalwächter, T. Thurn-Albrecht, M. Couty and J. Oberdisse, *ACS Macro Letters*, 2014, **3**, 448-452.

162 A. C. Genix, G. P. Baeza and J. Oberdisse, *Eur. Polym. J.*, 2016, **85**, 605-619.

163 D. Musino, A.-C. Genix, C. Fayolle, A. Papon, L. Guy, N. Meissner, R. Kozak, P. Weda, T. Bizien, T. Chaussée and J. Oberdisse, *Macromolecules*, 2017, **50**, 5138-5145.

164 D. Yamaguchi, T. Yuasa, T. Sone, T. Tominaga, Y. Noda, S. Koizumi and T. Hashimoto, *Macromolecules*, 2017, **50**, 7739-7759.

165 G. Beaucage, *J. Appl. Cryst.*, 1996, **29**, 134-146.

166 T. Koga, T. Hashimoto, M. Takenaka, K. Aizawa, N. Amino, M. Nakamura, D. Yamaguchi and S. Koizumi, *Macromolecules*, 2008, **41**, 453-464.

167 M. Takenaka, *Polymer Journal*, 2012, **45**, 10-19.

168 Y. Jin, G. Beaucage, K. Vogtt, H. Jiang, V. Kuppa, J. Kim, J. Ilavsky, M. Rackaitis, A. Mulderig, K. Rishi and V. Narayanan, *Polymer*, 2017, **129**, 32-43.

169 A. M. Vindedahl, J. H. Strehlau, W. A. Arnold and R. L. Penn, *Environmental Science: Nano*, 2016, **3**, 494-505.

170 C. Kästner, D. Lichtenstein, A. Lampen and A. F. Thünemann, *Colloids and Surfaces A: Physicochemical and Engineering Aspects*, 2017, **526**, 76-81.

TOC

Recent experimental approaches to inducing, controlling, and finally using nanoparticle aggregation are reviewed.